Optimum-pursuing method for constrained optimization and reliability-based design optimization problems using Kriging model

Meng, Zeng; Kong, Lin; Yi, Jiaxiang; Peng, Hao

Optimum-pursuing method for constrained optimization and reliability-based design optimization problems using Kriging model

Zeng Meng [a,b,*], Lin Kong [c], Jiaxiang Yi [d], Hao Peng [b,*]

[a] School of Civil Engineering, Hefei University of Technology, Hefei 230009, PR China
[b] Department of Engineering Mechanics, State Key Laboratory of Structural Analyses for Industrial Equipment, Dalian University of Technology, Dalian 116024, PR China
[c] Xi'an Modern Chemistry Research Institute, Xi'an 710065, PR China
[d] Material Science and Engineering, Delft University of Technology, Delft 2628CD, the Netherlands

HIGHLIGHTS

- An optimum-pursuing method is developed for constrained optimization and reliability-based design optimization problems.
- An optimum-pursuing function is proposed from the viewpoint of the optimization theory.
- The well-known U function is rigorously derived based on the proposed optimum-pursuing function.
- Optimum-pursuing method outperforms alternative methods in terms of both accuracy and efficiency.

ARTICLE INFO

ABSTRACT

This paper proposes a new active learning method named as optimum-pursuing method (OPM) from the viewpoint of optimization theory, which aims to provide an effective tool for solving constrained optimization and reliability-based design optimization (RBDO) problems with low computation cost. It uses the cheap Kriging metamodel to replace the expensive physical response. The novelty of the proposed OPM primarily lies in two aspects. First, the OPM utilizes the advantage of the optimization theory rather than sampling technology. By using the augmented Lagrangian approach, it comprehensively considers the objective, constraints, and their relations, thereby automatic identification of important region in the vicinity of the optimum. Second, the accordingly optimum-pursuing function consists of three parts: Kriging mean, Kriging standard deviation, and merit function. Also, the target reliability surface is further considered to enhance the local accuracy of the reliability analysis. The performance of OPM is tested for both deterministic optimization and problems, in which two mathematical and three real-world engineering examples are selected to showcase the feasibility and validity. The results demonstrate that OPM is promising for solving both deterministic optimization and RBDO problems by comparing with the well-known active learning methods.

* Corresponding authors at: School of Civil Engineering, Hefei University of Technology, Hefei 230009, PR China.
E-mail addresses: mengz@hfut.edu.cn (Z. Meng), haopeng@dlut.edu.cn (H. Peng).

1. Introduction

High computation efficiency, robustness, generalization, and accuracy are persistent pursuit for structural optimization design [1]. With the rapid development of powerful computer aided engineering technology, the optimization algorithm integrated with the finite element method becomes a popular way for real-world engineering system [2]. However, the complex engineering problems, such as large-scale problem, nonlinear problem, and dynamic problem, are time-consuming and always hard to be optimized practically [3–5].

Under this circumstance, the metamodel technology has emerged and demonstrated the strong vitality for optimization design [6, 7]. Nowadays, the widely used method includes the response surface method [8,9], Kriging model [10], support vector machine [11, 12], and neural network [13,14]. Recently, the data-driven method was also introduced in the optimization field [15–17]. Among them, the Kriging model has been widely employed, which contains two specific features [18,19]. First, Kriging model has interpolation property, which can accurately predict the response value at the design of experiment (DOE) [20]. Second, the Kriging metamodel can provide stochastic property and predict error at the unknown point [21]. Benefiting from the above advantages, the active learning technology was developed for Kriging model, which aims to add new points at the interested region, thereby promoting the computational efficiency and accuracy [22,23]. The active learning technology is regarded as a great progress, and the key is constructing the effectively active learning function [24,25]. Picheny et al. [19] presented a detailed investigation for active learning strategies. Their results indicated that the active learning strategies not only are insensitive to the initial sample size and Kriging parameters, but also significantly promote the efficiency. Until now, the active learning technology achieves huge success and is widely applied in the reliability analysis and optimization design fields [26,27].

The development of active learning technology can be traced back to the original work of Jones et al. [28], and the expected improvement (EI) function was developed by using the expect value of the improvement function to update the DOE. Subsequently, Osborne et al. [29] put forward the according active learning function under the Bayesian framework. Huang et al. [30] suggested an augmented EI function to accurately predict the stochastic responses. Picheny et al. [31] developed the expected quantile improvement method to reduce the computational time. Scott et al. [32] utilized the response gradient to sequentially determine the optimal sampling locations. Similarly, Chen et al. [33] combined the gradient and EI function to enhance the computational efficiency. Moreover, other active learning methods were constantly proposed, such as parallel computing method [34], minimal quantile criteria [35], informational approach [36], enhanced Kriging leave-one-out cross-validation [37], Kriging-assisted two-archive evolutionary algorithm [38], and Kriging-assisted teaching-learning-based optimization [39]. In general, the above-mentioned active learning methods are promising for settling the unconstrained optimization problem. However, it should be emphasized that the capacity of these methods is limited for settling the constrained optimization problem. Comparing with unconstrained optimization problem, the optimum always located around the constraint boundary (i.e. limit state function, LSF), and the Kriging model should simultaneously and accurately predict the objective, constraints, and their relations. Thus, it is a great challenging work. Juliani and Gomes [40] disclosed that the utilization of active learning method for generalized structural optimization problems were rarely found, and a three-stage strategy framework was suggested. Parr et al. [41] suggested the probability of feasibility (PoF) method, and the probability of improvement was employed. Zhou et al. [42] sequentially added the samples with the maximum predicted error to enhance the accuracy of Kriging model. Cheng et al. [43] adopted the lower confidence bounding (LCB) strategy to add the samples on the LSF. However, since the constrained optimization problem contains multiple responses, there are still huge difficulties for improving the predicted accuracy and efficiency by using the Kriging model [40].

In addition, it should be noted that there always exist many unavoidable random parameters in real-world engineering structures [44], so the reliability-based design optimization (RBDO) methodology emerges. The classic RBDO method employs the first-order reliability method for assessing the uncertain constraint and most probable target point (MPTP) efficiently and accurately, in which the reliability index approach [45], the performance measure approach (PMA) [46], and the sequential optimization and reliability assessment method [47] are representatives. Considering the high efficiency of Kriging, it is also extended into the RBDO field. However, unlike the deterministic optimization (DO) problem, the LSF of RBDO is the key. Therefore, many active learning methods are developed to approximate the LSF accurately and efficiently. Lee and Jung [48] made a promising attempt, and the constraint boundary sampling method was proposed accordingly. Subsequently, the expected feasibility method was further constructed by Bichon et al. [49,50], and its purpose is to effectively predict the LSF by using the Kriging mean, variance, and threshold value.

Subsequently, the improved active learning methods were constantly put forward. Echard et al. [25] constructed the typical U function, which used the ratio between the predicted value and standard deviation to add new samples around the LSF. Yang et al. [51] suggested the expected risk function (ERF) by minimizing the risk of LSF. Then, Xiao et al. [52] extended the ERF for solving the system RBDO problems successfully, in which the series and parallel constraints were considered. Similarly, the system active learning methods were reported by using the dependent Kriging prediction [53,54]. For example, Yang et al. [55] introduced the index function to distinguish the active and inactive constraints. Wang et al. [56] divided the entire region into the potential safety and failure domains, and the new samples only generated in the failure domain to improve the efficiency. Kroetz [57] et al. employed two adaptive coupled Kriging models to approximate the objective function and LSFs, respectively. Khorramian and Oudah [58] developed weighted Kriging occurrence, which simultaneously considers the probability of improvement and the density of DOE. Teixeira [59] applied density scanning to improve the efficiency of the adaptive Kriging. Meng et al. [60] predicted the LSF accurately by proposing the most probable learning function, and the single-loop technique was employed to accelerate the computation rate. Furthermore, Meng et al. [61] used the water cycle algorithm for improving the global convergence, in which the interval and random variables were simultaneously considered.

From the above review, it can be concluded that the Kriging model plays an important role for DO and RBDO, and the existing

methods are competitive. However, there are still some deficiencies. On the one hand, the existing works focus on separate dealing with objective function and constraint functions. However, the complex relationship among different functions and the contribution of these functions for optimum are vague. On the other hand, the RBDO simultaneously carries out the reliability analysis and optimization. Thus, the existing active learning methods tend to requiring a large number of samples for predicting LSF, which cannot identify the contribution of sample for the optimum, thereby incurring the highly computational cost.

To overcome the above drawbacks, this work proposes the optimum-pursuing method (OPM), in which both DO and RBDO problems are solved effectively. The optimum-pursuing function (OPF) is rigorously constructed from the viewpoint of the optimization theory. The organization of the paper is as below. Section 2 brief reviews the concept of DO, RBDO, and Kriging model. Section 3 describes the proposed OPM for DO, while Section 4 describes the OPM for RBDO. The relation between OPF and U function is discussed in Section 5. The test examples are shown in Section 6.

2. Overview for DO, RBDO, and Kriging

2.1. DO

The purpose of DO is to minimize the objective with the constraints [62]. Its formulation is mathematically stated as below:

$$
\begin{aligned}
& \text{find } \mathbf{x} = [x_1, x_2, ..., x_n] \\
& \min f(\mathbf{x}) \\
& s.t. g_i(\mathbf{x}) \leq 0, i = 1, ..., ng \\
& h_j(\mathbf{x}) = 0, j = 1, ..., nh \\
& \mathbf{x}^L \leq \mathbf{x} \leq \mathbf{x}^U
\end{aligned}
\tag{1}
$$

where $\mathbf{x}$ denotes the design variable vector. $\mathbf{x}^U$ and $\mathbf{x}^L$ denote the upper bounds and lower bounds, respectively. n denotes the dimension of $\mathbf{x}$. $f(\mathbf{x})$ denotes the objective function. ng denotes the inequality constraint number. nh denotes the equality constraint number.

2.2. RBDO

The main difference between DO and RBDO is that the RBDO is constructed based on the uncertain hypothesis [63,64]. The RBDO approach uses the probabilistic constraint to ensure the safety level. Its formulation is as follows:

$$
\begin{aligned}
& \text{find } \boldsymbol{\mu}_{\mathbf{x}} = \left[\mu_{x_1}, \mu_{x_2}, ..., \mu_{x_n}\right] \\
& \min f(\boldsymbol{\mu}_{\mathbf{x}}) \\
& s.t. \text{Prob}(g_i(\mathbf{x}) \leq 0) \leq \Phi\left(-\beta_i^t\right), i = 1, ..., ng \\
& \boldsymbol{\mu}_{\mathbf{x}}^L \leq \boldsymbol{\mu}_{\mathbf{x}} \leq \boldsymbol{\mu}_{\mathbf{x}}^U
\end{aligned}
\tag{2}
$$

where $\mathbf{x}$ denotes the random variable vector. $\boldsymbol{\mu}_{\mathbf{x}}$ is the accordingly mean vector. Prob denotes the reliability operator. β_i^t denotes the target reliability index. Φ denotes the standard normal cumulative density function.

2.3. Kriging

Kriging is a popular metamodel, which is commonly employed to accelerate the optimization and reliability computation speed [65,66]. It is composed by a polynomial term and a stochastic term, which is stated as

$$
\widehat{g}(\mathbf{x}) = \mathbf{h}^T(\mathbf{x})\boldsymbol{\gamma} + v(\mathbf{x})
\tag{3}
$$

where $\widehat{g}(\mathbf{x})$ denotes the predicted response with variables x. $\mathbf{h}(\mathbf{x})$ refers to the basis vector. $\boldsymbol{\gamma}$ refers to the regression coefficient vector. The stochastic term $v(\mathbf{x})$ obeys a stationary Gaussian process. Its mean is zero, while the covariance between arbitrary points is depicted by

$$
\text{Cov}\left(v(\mathbf{x}_i), v(\mathbf{x}_j)\right) = \sigma_v^2 R_v(\mathbf{x}_i, \mathbf{x}_j) i, j = 1, 2, ..., k
\tag{4}
$$

where Cov denotes the covariance. σ_v^2 refers to the variance of $v(\mathbf{x})$. $R_v(\mathbf{x}_i, \mathbf{x}_j)$ is the correlation function, where the Gaussian function is widely employed. It is stated as follows:

$$
R_v(\mathbf{x}_i, \mathbf{x}_j) = \prod_{l=1}^{n} \exp\left(-\theta_l\left(x_i^l - x_j^l\right)^2\right)
\tag{5}
$$

where θ_l represents the correlation parameter that is determined by the maximum likelihood method.

$$L(\boldsymbol{\theta}) = \left(2\pi\sigma_v^2\right)^{-\frac{k}{2}}|\mathbf{R}|^{-\frac{1}{2}}\exp\left(-\frac{k}{2}\right) \tag{6}$$

where $\mathbf{R}$ denotes correlation matrix, and its component is $R_v(\mathbf{x}_i, \mathbf{x}_j)$. The regression coefficients and the approximate variance are computed by

$$\widehat{\gamma} = \left(\mathbf{H}^T\mathbf{R}^{-1}\mathbf{H}\right)^{-1}\mathbf{H}^T\mathbf{R}^{-1}\mathbf{g} \tag{7}$$

$$\widehat{\sigma}_v^2 = \frac{1}{k}(\mathbf{g} - \mathbf{H}\widehat{\gamma})^T\mathbf{R}^{-1}(\mathbf{g} - \mathbf{H}\widehat{\gamma}) \tag{8}$$

For an arbitrary prediction point $\mathbf{x}_0$, the correlation $\mathbf{r}_0 = [R(\mathbf{x}_0, \mathbf{x}_1), \dots, R(\mathbf{x}_0, \mathbf{x}_k)]$ is constructed. Then, the unbiased predictor $\widehat{\mu}_{\hat{g}(\mathbf{x}_0)}$ and Kriging variance $\widehat{\sigma}_{\hat{g}(\mathbf{x}_0)}^2$ are evaluated by

$$\begin{aligned}
\widehat{\mu}_{\hat{g}(\mathbf{x}_0)} &= \mathbf{h}^T(\mathbf{x}_0)\widehat{\gamma} + \mathbf{r}_0^T\mathbf{R}^{-1}(\mathbf{g} - \mathbf{H}\widehat{\gamma}) \\
\widehat{\sigma}_{\hat{g}(\mathbf{x}_0)}^2 &= \widehat{\sigma}_v^2\left(1 + \mathbf{u}^T\left(\mathbf{H}^T\mathbf{R}^{-1}\mathbf{H}\right)^{-1}\mathbf{u} - \mathbf{r}_0^T\mathbf{R}^{-1}\mathbf{r}_0\right)
\end{aligned} \tag{9}$$

where $\mathbf{u} = \mathbf{H}^T\mathbf{R}^{-1}\mathbf{r}_0 - \mathbf{h}(\mathbf{x}_0)$. To establish the Kriging model and predict the response simply, the Kriging toolbox DACE is employed in this study [67].

3. The OPM for DO

Unlike other surrogate models, Kriging exhibits the unique superiority owing to the active learning behavior, which can sequentially add the samples in the interested region. Note that the complex optimization problem always contains multiple structural responses, and how to cooperatively deal with the objective and constraint functions is confronted with enormous challenge. On the one hand, the optimum has the small objective function value, while the optimum is located in the safe region. On the other hand, the Kriging models of objective and constraint functions have predicted errors. In order to simultaneously consider the objective and constraint functions, the numerical optimization methods can be employed. It was reported that the external penalization approach is an effectively numerical optimization method, which is regarded as a standard tool in optimization [68,69]. Its basic idea is to transform a constrained problem into an unconstrained problem. However, the convergence of external penalization approach is only guaranteed when the penalization parameters are infinity. To address this numerical issue, the augmented Lagrangian approach [70, 71] is further proposed. Based on augmented Lagrangian approach, we can construct the following augmented Lagrangian function for DO model of Eq. (1).

$$M = f(\mathbf{x}) + \sum_{i=1}^{ng}\left[\lambda_i^{(m)}\psi_i(\mathbf{x}) + \frac{r^{(m)}}{2}\psi_i(\mathbf{x})^2\right] + \sum_{j=1}^{nh}\left[\lambda_{j+ng}^{(m)}h_j(\mathbf{x}) + \frac{r^{(m)}}{2}h_j(\mathbf{x})^2\right] \tag{10}$$

where

$$\psi_i(\mathbf{x}) = \max\left[g_i(\mathbf{x}), -\frac{\lambda_i^{(m)}}{r^{(m)}}\right] \tag{11}$$

where $\lambda_i^{(m)}$ is the ith Lagrange multiplier estimator, and $r^{(m)}$ is a quadratic penalty factor. $\lambda_i^{(m)}$ and $r^{(m)}$ should be updated during the optimization process, and their initial values are 0 and 10 in this paper. According to the works of [70,71], the penalty factor $r^{(m)}$ and Lagrange multiplier estimator $\lambda_i^{(m)}$ are typically updated as

$$r^{(m+1)} = \min\left[\alpha r^{(m)}, r_{\max}\right] \tag{12}$$

$$\lambda_i^{(m+1)} = \lambda_j^{(m)} + r^{(m)}\psi_i(\mathbf{x}) \tag{13}$$

where α is an update parameter, and $r_{\max}$ is an upper limit that is used to prevent numerical instabilities. $\alpha = 1.1$ and $r_{\max} = 1000$ are employed in this work.

Based on the augmented Lagrangian approach, the minimization of Eq. (1) can be converted into the minimization of Eq. (10). Then, we can combine the different response functions together. Once the establishment of Kriging model completes, the optimization model is stated as follows:

$$\widehat{M} = \widehat{f}(\mathbf{x}) + \sum_{i=1}^{ng}\left[\lambda_i^{(m)}\widehat{\psi}_i(\mathbf{x}) + \frac{r^{(m)}}{2}\widehat{\psi}_i(\mathbf{x})^2\right] + \sum_{j=1}^{nh}\left[\lambda_{j+ng}^{(m)}\widehat{h}_j(\mathbf{x}) + \frac{r^{(m)}}{2}\widehat{h}_j(\mathbf{x})^2\right] \tag{14}$$

where

$$\widehat{\psi}_i(\mathbf{x}) = \max\left[\widehat{g}_i(\mathbf{x}), -\frac{\lambda_i^{(m)}}{r^{(m)}}\right] \tag{15}$$

For solving Eq. (14), there are two different situations. When the Kriging model provides sufficient accuracy, the optimum computed by the Kriging model is close to the real optimum. On the contrary, when the Kriging model is inaccurate, the optimum may locate in the region with large Kriging variance. Therefore, we propose the OPM, which uses the reciprocals of coefficient of variation as the active learning function. If the mean of Kriging merit function of Eq. (14) is minimized, it achieves the optimum of current Kriging optimization problem. If the standard deviation (SD) of Kriging merit function of Eq. (14) is small, it means the predicted error of Kriging optimization model is minimized. Therefore, we should minimize the mean and maximize the SD to add the samples with small value of Kriging merit function and large predicted error. In this way, the concerned region can be quickly identified, and the new sample is added in the vicinity of the optima. Then, the precision of the Kriging model can be constantly enhanced through sequential adding new samples. Therefore, the proposed OPM focuses on finding a good local approximation in the region around the optimum, thereby avoiding generating too many points in the global region. In general, the mean and variance of Eq. (14) are

$$
\begin{aligned}
\mu(\widehat{M}) &= \mu\left(\widehat{f}(\mathbf{x}) + \sum_{i=1}^{ng}\left[\lambda_i^{(m)}\widehat{\psi}_i(\mathbf{x}) + \frac{r^{(m)}}{2}\widehat{\psi}_i(\mathbf{x})^2\right] + \sum_{j=1}^{nh}\left[\lambda_{j+ng}^{(m)}\widehat{h}_j(\mathbf{x}) + \frac{r^{(m)}}{2}\widehat{h}_j(\mathbf{x})^2\right]\right) \\
&= \mu_{\widehat{f}(\mathbf{x})} + \sum_{i=1}^{ng}\left[\lambda_i^{(m)}\mu_{\widehat{\psi}_i(\mathbf{x})} + \frac{r^{(m)}}{2}\left(\mu_{\widehat{\psi}_i(\mathbf{x})}^2 + \sigma_{\widehat{\psi}_i(\mathbf{x})}^2\right)\right] + \sum_{j=1}^{nh}\left[\lambda_{j+ng}^{(m)}\mu_{\widehat{h}_j(\mathbf{x})} + \frac{r^{(m)}}{2}\left(\mu_{\widehat{h}_j(\mathbf{x})}^2 + \sigma_{\widehat{h}_j(\mathbf{x})}^2\right)\right]
\end{aligned}
\tag{16}
$$

$$
\begin{aligned}
Var(\widehat{M}) &= Var\left(\widehat{f}(\mathbf{x}) + \sum_{i=1}^{ng}\left[\lambda_i^{(m)}\widehat{\psi}_i(\mathbf{x}) + \frac{r^{(m)}}{2}\widehat{\psi}_i(\mathbf{x})^2\right] + \sum_{j=1}^{nh}\left[\lambda_{j+ng}^{(m)}\widehat{h}_j(\mathbf{x}) + \frac{r^{(m)}}{2}\widehat{h}_j(\mathbf{x})^2\right]\right) \\
&= Var(\widehat{f}(\mathbf{x})) + \sum_{i=1}^{ng}Var\left[\lambda_i^{(m)}\widehat{\psi}_i(\mathbf{x}) + \frac{r^{(m)}}{2}\widehat{\psi}_i(\mathbf{x})^2\right] + \sum_{j=1}^{nh}Var\left[\lambda_{j+ng}^{(m)}\widehat{h}_j(\mathbf{x}) + \frac{r^{(m)}}{2}\widehat{h}_j(\mathbf{x})^2\right] \\
&\quad + 2\sum_{i=1}^{ng}Cov\left[\widehat{f}(\mathbf{x}), \lambda_i^{(m)}\widehat{\psi}_i(\mathbf{x}) + \frac{r^{(m)}}{2}\widehat{\psi}_i(\mathbf{x})^2\right] + 2\sum_{j=1}^{nh}Cov\left[\widehat{f}(\mathbf{x}), \lambda_{j+ng}^{(m)}\widehat{h}_j(\mathbf{x}) + \frac{r^{(m)}}{2}\widehat{h}_j(\mathbf{x})^2\right] \\
&\quad + \sum_{i=1}^{ng}\sum_{\underset{=}{j}}^{ng}Cov\left[\lambda_i^{(m)}\widehat{\psi}_i(\mathbf{x}) + \frac{r^{(m)}}{2}\widehat{\psi}_i(\mathbf{x})^2, \lambda_j^{(m)}\widehat{\psi}_j(\mathbf{x}) + \frac{r^{(m)}}{2}\widehat{\psi}_j(\mathbf{x})^2\right] \\
&\quad + \sum_{i=1}^{nh}\sum_{\underset{=}{j}}^{nh}Cov\left[\lambda_{i+ng}^{(m)}\widehat{h}_i(\mathbf{x}) + \frac{r^{(m)}}{2}\widehat{h}_i(\mathbf{x})^2, \lambda_{j+ng}^{(m)}\widehat{h}_j(\mathbf{x}) + \frac{r^{(m)}}{2}\widehat{h}_j(\mathbf{x})^2\right] \\
&\quad + 2\sum_{i=1}^{ng}\sum_{j=1}^{nh}Cov\left[\lambda_i^{(m)}\widehat{\psi}_i(\mathbf{x}) + \frac{r^{(m)}}{2}\widehat{\psi}_i(\mathbf{x})^2, \lambda_{j+ng}^{(m)}\widehat{h}_j(\mathbf{x}) + \frac{r^{(m)}}{2}\widehat{h}_j(\mathbf{x})^2\right]
\end{aligned}
\tag{17}
$$

The covariance between the separately established Kriging models is 0, and the derivation process can be seen in the Appendix. However, when the functions are constructed by the same Kriging model, the covariance should be considered. Therefore, $Var(\widehat{M})$ can be simplified as follows:

$$
\begin{aligned}
Var(\widehat{M}) &= Var\left(\widehat{f}(\mathbf{x}) + \sum_{i=1}^{ng}\left[\lambda_i^{(m)}\widehat{\psi}_i(\mathbf{x}) + \frac{r^{(m)}}{2}\widehat{\psi}_i(\mathbf{x})^2\right] + \sum_{j=1}^{nh}\left[\lambda_{j+ng}^{(m)}\widehat{h}_j(\mathbf{x}) + \frac{r^{(m)}}{2}\widehat{h}_j(\mathbf{x})^2\right]\right) \\
&= Var(\widehat{f}(\mathbf{x})) + \sum_{i=1}^{ng}Var\left[\lambda_i^{(m)}\widehat{\psi}_i(\mathbf{x}) + \frac{r^{(m)}}{2}\widehat{\psi}_i(\mathbf{x})^2\right] + \sum_{j=1}^{nh}Var\left[\lambda_{j+ng}^{(m)}\widehat{h}_j(\mathbf{x}) + \frac{r^{(m)}}{2}\widehat{h}_j(\mathbf{x})^2\right]
\end{aligned}
\tag{18}
$$

where

$$
\begin{aligned}
&Var\left[\lambda_i^{(m)}\widehat{\psi}_i(\mathbf{x}) + \frac{r^{(m)}}{2}\widehat{\psi}_i(\mathbf{x})^2\right] \\
&= Var\left[\lambda_i^{(m)}\widehat{\psi}_i(\mathbf{x})\right] + Var\left[\frac{r^{(m)}}{2}\widehat{\psi}_i(\mathbf{x})^2\right] + 2Cov\left[\lambda_i^{(m)}\widehat{\psi}_i(\mathbf{x}), \frac{r^{(m)}}{2}\widehat{\psi}_i(\mathbf{x})^2\right] \\
&= \left(\lambda_i^{(m)}\right)^2\sigma_{\widehat{\psi}_i(\mathbf{x})}^2 + \left(\frac{r^{(m)}}{2}\right)^2\left(2\sigma_{\widehat{\psi}_i(\mathbf{x})}^4 + 4\sigma_{\widehat{\psi}_i(\mathbf{x})}^2\mu_{\widehat{\psi}_i(\mathbf{x})}^2\right) + \lambda_i^{(m)}r^{(m)}\left(2\sigma_{\widehat{\psi}_i(\mathbf{x})}^2\mu_{\widehat{\psi}_i(\mathbf{x})} + \sigma_{\widehat{\psi}_i(\mathbf{x})}^3\right)
\end{aligned}
\tag{19}
$$

Table 1
Pseudo code of the OPM.

Step	Description
1	Define the design variables $\mathbf{x}$, allowable error ε_t, initial iterative step $k=0$, and maximum iterative number t.
2	Generate the initial DOE based on LHS. Construct the Kriging model using the initial DOE.
3	While $k<t$ and $\varepsilon<\varepsilon_t$
4	$k=k+1$
5	The objective function is computed based on the Eq. (24).
6	Define the initial Lagrange multiplier estimator $\lambda^{(0)}$, initial quadratic penalty factor $r^{(0)}$, initial iterative step $m=0$, and maximum iterative number t_m.
7	While $m<t_m$
8	$m=m+1$
9	Perform the PSO algorithm to update $\mathbf{x}_k^{(m)}$.
10	Update $r^{(m)}$ and $\lambda^{(m)}$ every 5 iterative steps.
11	End
12	Add the best solution $\mathbf{x}_k^{'}$ into the DOE.
13	Update the Kriging model based on the existing DOE.
14	Compute the maximum relative error at the best solution $\mathbf{x}_k^{'}$.
15	Perform the DO to obtain the current optimum $\mathbf{x}^*$.
16	End
17	Output the optimum $\mathbf{x}^*$.

$$
Var\left[\lambda_j^{(m)}\widehat{h}_j(\mathbf{x}) + \frac{r^{(m)}}{2}\widehat{h}_j(\mathbf{x})^2\right]
$$

$$
= Var\left[\lambda_j^{(m)}\widehat{h}_j(\mathbf{x})\right] + Var\left[\frac{r^{(m)}}{2}\widehat{h}_j(\mathbf{x})^2\right] + 2Cov\left[\lambda_j^{(m)}\widehat{h}_j(\mathbf{x}), \frac{r^{(m)}}{2}\widehat{h}_j(\mathbf{x})^2\right] \tag{20}
$$

$$
= \left(\lambda_j^{(m)}\right)^2\sigma_{\hat{h}_j(\mathbf{x})}^2 + \left(\frac{r^{(m)}}{2}\right)^2\left(2\sigma_{\hat{h}_j(\mathbf{x})}^4 + 4\sigma_{\hat{h}_j(\mathbf{x})}^2\mu_{\hat{h}_j(\mathbf{x})}^2\right) + \lambda_j^{(m)}r^{(m)}\left(2\sigma_{\hat{h}_j(\mathbf{x})}^2\mu_{\hat{h}_j(\mathbf{x})} + \sigma_{\hat{h}_j(\mathbf{x})}^3\right)
$$

where $\mu_{\hat{\psi}_i(\mathbf{x})}$ and $\sigma_{\hat{\psi}_i(\mathbf{x})}^2$ are computed by

$$
\mu_{\hat{\psi}_i(\mathbf{x})} = \begin{cases} -\dfrac{\lambda_i^{(m)}}{r^{(m)}} \; if\, \widehat{g}_i(\mathbf{x}) < -\dfrac{\lambda_i^{(m)}}{r^{(m)}} \\[4mm] \mu_{\hat{g}_i(\mathbf{x})} \; if\, \widehat{g}_i(\mathbf{x}) \geq -\dfrac{\lambda_i^{(m)}}{r^{(m)}} \end{cases} \tag{21}
$$

$$
\sigma_{\hat{\psi}_i(\mathbf{x})}^2 = \begin{cases} 0 \; if\, \widehat{g}_i(\mathbf{x}) < -\dfrac{\lambda_i^{(m)}}{r^{(m)}} \\[4mm] \sigma_{\hat{g}_i(\mathbf{x})}^2 \; if\, \widehat{g}_i(\mathbf{x}) \geq -\dfrac{\lambda_i^{(m)}}{r^{(m)}} \end{cases} \tag{22}
$$

Then, the optimum-pursuing function (OPF) of OPM is constructed as below:

$$
OPF_1 = \frac{\mu(\widehat{M})}{\sqrt{Var(\widehat{M})}} \tag{23}
$$

Although the OPF is capable of providing accurate results, the fractional form encounters numerical issues, thereby preventing rapid convergence. Inspired by the active weight learning function [72], the OPF is formulated as the sum of $\mu(\widehat{M})$ and $1/\sqrt{Var(\widehat{M})}$ to address the numerical issues. Moreover, when the Kriging model is accurate, the value of $Var(\widehat{M})$ is very small, thereby leading to an exceptionally large value of $1/\sqrt{Var(\widehat{M})}$. In this context, the term $\mu(\widehat{M})$ in the OPF does not work, which results in the numerical issues. Thus, $\min(1/\sqrt{Var(\widehat{M})}, 10\cdot\mu(\widehat{M}))$ is introduced to impose an upper limit on the term $1/\sqrt{Var(\widehat{M})}$ to overcome the numerical issue. Furthermore, the sum of $\mu(\widehat{M})$ and $\min(1/\sqrt{Var(\widehat{M})}, 10\cdot\mu(\widehat{M}))$ is used to improve the stability, and the OPF is stated as below:

$$
OPF_2 = \mu(\widehat{M}) + \min\left(1/\sqrt{Var(\widehat{M})}, 10\cdot\mu(\widehat{M})\right) \tag{24}
$$

Like other active learning methods, there are two different ways to update the DOE by using the OPF. The first way is using the sampling strategy, e.g. Latin hypercube sampling (LHS), in which the minimization value of OPF is selected as the new DOE sample. The second way is using optimization strategy, and the new samples are sequentially added in DOE. In general, the new sample is

determined by solving the following optimization formulation:

$$
\begin{aligned}
&\text{find } \mathbf{x}'_k \\
&\min OPF_2(\mathbf{x}_k)
\end{aligned}
\tag{25}
$$

where $\mathbf{x}'_k$ is the best solution of Eq. (25). When the $\mathbf{x}'_k$ is obtained by using the optimization algorithm, it can be added into the DOE to improve the computational accuracy. In this paper, the particle swarm optimization (PSO) method is utilized, in which the maximum number of generations is set as 250. The pseudo code of OPM is listed in Table 1.

In addition, it should be emphasized that the covariance is not equal to the 0 when the objective and constraint functions are co-established. In this way, the neglect of the covariance leads to computational errors. However, the errors induced by this perturbation are small due to the stability of the active learning methods. Therefore, it can also be regarded as a reasonable approximation.

4. The OPM for RBDO

4.1. OPM for computing MPTP

It is reported that PMA is one promising RBDO method, which is widely employed in different fields, e.g. aerospace, mechanics, and vehicle engineering industries [73,74]. The PMA converts the probabilistic constraint to an optimization model, and the accordingly RBDO model contains double optimization loops. Its key is to search the MPTP in the inner loop, which is stated as

$$
\begin{aligned}
&\text{find } \mathbf{u} \\
&\min \ g_i \\
&\text{s.t.} \ \parallel \mathbf{u} \parallel = \beta^t
\end{aligned}
\tag{26}
$$

where $\mathbf{u}$ are the standard normal variables that are obtained from random variables $\mathbf{x}$ by using the Rosenblatt transformation [75,76]. g_i is the ith performance function. Its augmented Lagrangian function based on Kriging model is stated as below:

$$
\widehat{M}_{MPTP} = \widehat{g}_i + \lambda^{(m)}(\parallel \mathbf{u} \parallel - \beta^t) + \frac{r^{(m)}}{2}(\parallel \mathbf{u} \parallel - \beta^t)^2
\tag{27}
$$

Considering $\sigma(\parallel \mathbf{u} \parallel) = 0$ and $\sigma(\beta^t) = 0$, its mean and variance are stated as below:

$$
\mu(\widehat{M}_{MPTP}) = \mu_{\widehat{g}_i} + \lambda^{(m)}(\parallel \mathbf{u} \parallel - \beta^t) + \frac{r^{(m)}}{2}(\parallel \mathbf{u} \parallel - \beta^t)^2
\tag{28}
$$

$$
Var(\widehat{M}_{MPTP}) = Var\left(\widehat{g}_i + \lambda^{(m)}(\parallel \mathbf{u} \parallel - \beta^t) + \frac{r^{(m)}}{2}(\parallel \mathbf{u} \parallel - \beta^t)^2\right) = \sigma_{\widehat{g}_i}^2
\tag{29}
$$

Then, the OPF for computing the MPTP is as follows:

$$
OPF_{MPTP} = \mu(\widehat{M}_{MPTP}) + \min\left(1 \left/ \sqrt{Var(\widehat{M}_{MPTP})}, 10 \cdot \mu(\widehat{M}_{MPTP})\right.\right)
\tag{30}
$$

Through optimizing the OPF_{MPTP}, the new sample can be obtained. The optimization formulation is stated as follows:

$$
\begin{aligned}
&\text{find } \mathbf{u}'_{k_2} \\
&\min OPF_{MPTP}(\mathbf{u}_{k_2})
\end{aligned}
\tag{31}
$$

where $\mathbf{u}'_{k_2}$ is the best solution of Eq. (31), and it is added into the DOE to improve the accuracy of MPTP computation.

4.2. OPM for PMA

For RBDO model with multiple constraints, the MPTP of active constraint is located at the LSF, i.e. $g_i(\mathbf{u}_{MPTP}) = 0$. Besides, the objective value of optimum is lower than that of other points in the safe region. In general, the outer loop of PMA is

$$
\begin{aligned}
&\text{find } \mathbf{x} = [x_1, x_2, ..., x_n] \\
&\min f(\mathbf{x}) \\
&s.t. G_i(\mathbf{x}) \le 0, i = 1, ..., ng \\
&\mathbf{x}^L \le \mathbf{x} \le \mathbf{x}^U
\end{aligned}
\tag{32}
$$

where the performance functions $G_i(\mathbf{x})$ and $g_i(\mathbf{u})$ satisfy the relation $G_i(\mathbf{x}) = -g_i(\mathbf{u})$. The augmented Lagrangian function is expressed as below:

$$
\widehat{M}_{PMA} = \widehat{f} + \sum_{i=1}^{ng}\left[\lambda_i^{(m)}\widehat{\psi}_i(\mathbf{x}) + \frac{r^{(m)}}{2}\widehat{\psi}_i(\mathbf{x})^2\right]
\tag{33}
$$

By neglecting the equality constraint for DO in Eqs. (14)–(24), we can obtain the OPF in the same way.
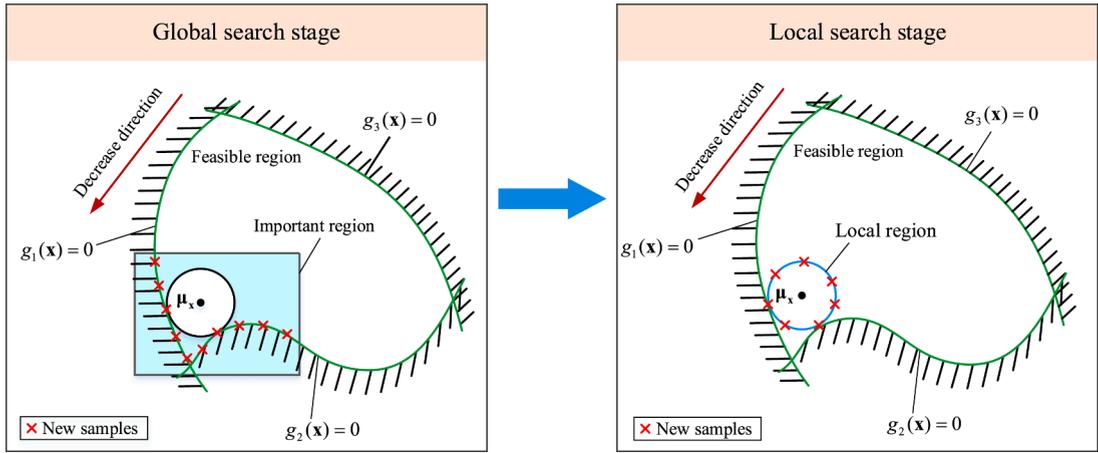
Fig. 1. Schematic diagram of AOPM.

$$OPF_{PMA} = \mu(\widehat{M}_{PMA}) + \min\left(1 \Big/ \sqrt{Var(\widehat{M}_{PMA})}, 10 \cdot \mu(\widehat{M}_{PMA})\right) \tag{34}$$

where

$$\mu(\widehat{M}_{PMA}) = \mu_{\hat{f}(\mathbf{x})} + \sum_{i=1}^{ng}\left[\lambda_i^{(m)}\mu_{\hat{\psi}_i(\mathbf{x})} + \frac{r^{(m)}}{2}\left(\mu_{\hat{\psi}_i(\mathbf{x})}^2 + \sigma_{\hat{\psi}_i(\mathbf{x})}^2\right)\right] \tag{35}$$

$$Var(\widehat{M}_{PMA}) = \sigma_{\hat{f}(\mathbf{x})}^2 + \sum_{i=1}^{ng} Var\left[\lambda_i^{(m)}\hat{\psi}_i(\mathbf{x}) + \frac{r^{(m)}}{2}\hat{\psi}_i(\mathbf{x})^2\right] \tag{36}$$

where $Var\left[\lambda_i^{(m)}\hat{\psi}_i(\mathbf{x}) + \frac{r^{(m)}}{2}\hat{\psi}_i(\mathbf{x})^2\right]$ can be computed by Eq. (19). Through minimizing the OPF_{PMA}, the new sample can be obtained. The optimization formulation is stated as follows:

$$\begin{aligned} &\text{find } \mathbf{x}'_{k_1}\\ &\min OPF_{PMA}(\mathbf{x}_{k_1}) \end{aligned} \tag{37}$$

where $\mathbf{x}'_{k_1}$ is the best solution of Eq. (37), and it is added into the DOE to update the Kriging model.

4.3. Augmented optimum-pursuing method

It should be noted that PMA consists of double optimization loops. The OPF of Eq. (34) can accurately predict the LSF around the optimum. However, it is constructed based on the outer loop of PMA, which neglects the impact of inner loop/MPTP search. Thus, when highly nonlinear and high-dimensional problems involve, it may generate unaccepted error. To enhance the local accuracy, the augmented optimum-pursuing method (AOPM) is further proposed, which combines the merits of OPM using MPTP and PMA.

The proposed AOPM consists of two stages: the global search stage and the local search stage, and the schematic diagram is illustrated in Fig. 1. The global search stage uses the OPM of PMA, which aims to find the important region around the optimum. Then, the PMA is carried out to approximate the optimum, and the computational error of the optimum should be checked. If the accuracy is high, it means the optimum is satisfactory and the local search stage is used to computing the MPTP. If the accuracy is low, the OPM of PMA should be used to improve the accuracy. In the local search stage, the OPM of MPTP is carried out to generate new samples, and the DOE is updated accordingly. Then, the PMA based on Kriging is performed, and the new optimum is found. In this way, the new samples are added sequentially, and the optimum is updated until achieving the accuracy requirement. In AOPM, the accuracy checking criterion is crucial. Since there are multiple objective and constraint functions in RBDO model, their accuracies should be simultaneously considered. Thus, the maximum relative errors of objective and constraint functions are checked at the updated point, and the accuracy checking criterion is stated as below:

$$\varepsilon_{\max} \leq \varepsilon_t \tag{38}$$

where ε_t is the allowable relative error that is 10^{-3} in this work. $\varepsilon_{\max}$ is as follows:

$$\varepsilon_{\max} = \max\left\{\frac{|f - \widehat{f}|}{|f| + \delta}, \frac{|g_1 - \widehat{g}_1|}{|g_1| + \delta}, \frac{|g_2 - \widehat{g}_2|}{|g_2| + \delta}, ..., \frac{|g_{ng} - \widehat{g}_{ng}|}{|g_{ng}| + \delta}\right\} \tag{39}$$

Table 2
Pseudo code of the AOPM for RBDO.

Step	Description
1	Perform the global search stage. Define the random variables $\mathbf{x}$, allowable error ε_t, initial iterative step $k_1=0$, and maximum iterative number t_1.
2	Generate the initial DOE based on LHS. Establish the Kriging model by using the initial DOE. Perform the global search stage.
3	While $k_1<t_1$ and $\varepsilon<\varepsilon_t$
4	$k_1=k_1+1$
5	The objective function is computed according to the Eq. (34).
6	Define the initial Lagrange multiplier estimator $\lambda^{(0)}$, initial quadratic penalty factor $r^{(0)}$, initial iterative step $m_1=0$, and maximum iterative number t_{m1}.
7	While $m_1<t_{m1}$
8	$m_1=m_1+1$
9	Perform the PSO algorithm to update $\mathbf{x}_{k_1}^{(m_1)}$.
10	Update $r^{(m_1)}$ and $\lambda^{(m_1)}$ every 5 iterative steps.
11	End
12	Add the best solution $\mathbf{x}'_{k_1}$ into the DOE.
13	Update the Kriging model based on the existing DOE.
14	Compute the maximum relative error based on the Eq. (39). Check the accuracy based on the Eq. (38).
15	Perform the RBDO to obtain the current optimum $\mathbf{x}^*$.
16	end
17	Perform the local search stage. Define the initial iterative step $k_2=0$ and maximum iterative number t_2.
18	While $k_2<t_2$ and $\varepsilon_2<\varepsilon_t$
19	$k_2=k_2+1$
20	The objective function is evaluated based on the Eq. (30).
21	Transform $\mathbf{x}_{k_2}$ into $\mathbf{u}_{k_2}$ by Rosenblatt transformation.
22	Define the initial Lagrange multiplier estimator $\lambda^{(0)}$, initial quadratic penalty factor $r^{(0)}$, initial iterative step $m_2=0$, and maximum iterative number t_{m2}.
23	While $m_2<t_{m2}$
24	$m_2=m_2+1$
25	Perform the PSO algorithm to update $\mathbf{u}_{k_2}^{(m_1)}$.
26	Update $r^{(m_2)}$ and $\lambda^{(m_2)}$ every 5 iterative steps.
27	End
28	Transform the best solution $\mathbf{u}'_{k_2}$ into $\mathbf{x}'_{k_2}$ by using the Rosenblatt transformation.
29	Add the sample $\mathbf{x}'_{k_2}$ into the existing DOE.
30	Update the Kriging model based on the existing DOE.
31	Compute the maximum relative error based on the Eq. (39). Check the accuracy based on the Eq. (38).
32	Perform the RBDO to obtain the current optimum $\mathbf{x}^*$.
33	End
34	Output the optimum $\mathbf{x}^*$.

where δ is a small positive value that is selected as 10^{-3}. It is utilized to prevent the singularity when f or g_i is equal to zero. Once the accuracy checking criterion is constructed, we can test the error at optimum.

4.4. Flowchart of AOPM

Table 2 summarizes the pseudo code of the AOPM for RBDO. The computation process is composed by a two-stage optimization loop.

5. Relation between OPF and U function

The U function is a popular active learning function [25], which is widely applied in the reliability computation owing to the simplicity and validity [24,77]. However, there is a lack of theoretical derivation process. Here we rigorously derive the U function based on the OPM and failure probability. In general, the failure probabilities based on the real performance function $g(\mathbf{x})$ and Kriging performance function $\widehat{g}(\mathbf{x})$ are stated as below:

$$P_f = \int \cdots \int_{g(\mathbf{x})<0} f(\mathbf{x})\mathrm{d}x_1\ldots\mathrm{d}x_n \tag{40}$$

$$\widehat{P}_f = \int \cdots \int_{\widehat{g}(\mathbf{x})<0} f(\mathbf{x})\mathrm{d}x_1\ldots\mathrm{d}x_n \tag{41}$$

where P_f and $\widehat{P}_f$ denote the failure probabilities with respect to $g(\mathbf{x})$ and $\widehat{g}(\mathbf{x})$, respectively. $f(\mathbf{x})$ represents the probability density function. From Eqs. (40) and (41), it can be found that the $P_f = \widehat{P}_f$ when $g(\mathbf{x}) = \widehat{g}(\mathbf{x})$. Therefore, we can construct the following optimization formulation to minimize the computation error between P_f and $\widehat{P}_f$.

Table 3
Results of example 1.

Methods	Objective	Design variables	F-evaluations	Error
DO				
MMA	0.8871	(2.9710,3.4036)	138	—
PoF	0.8870	(2.9741,3.4000)	41	5.6031×10^{-5}
MAX-MSE	0.8876	(2.9709,3.4034)	68	2.7216×10^{-4}
LCB	0.8885	(2.9913,3.3784)	45	3.2437×10^{-4}
OPM	0.8871	(2.9711,3.4036)	26	2.9284×10^{-6}
RBDO				
PMA	1.3038	(2.8162,3.2770)	231	—
SLA	1.3038	(2.8162,3.2770)	132	—
LHS	1.3041	(2.8161,3.2770)	100	0.6844
U	1.3042	(2.8233,3.2613)	57	6.7814×10^{-3}
ERF	1.3032	(2.8156,3.2782)	76	3.3306×10^{-4}
OPM	1.3038	(2.8163,3.2769)	29	6.1698×10^{-6}

$$\begin{aligned} &\text{find } \mathbf{x} = [x_1, x_2, \cdots, x_n] \\ &\min \varepsilon = |g(\mathbf{x}) - \widehat{g}(\mathbf{x})| \end{aligned} \tag{42}$$

where ε denotes the absolute error. When ε is zero, it means the Kriging performance function can provide satisfactory accuracy. It should be emphasized that this optimization problem is only a special case of Eq. (1), in which the mean and variance of ε are

$$\mu(\varepsilon) = \mu(|g(\mathbf{x}) - \widehat{g}(\mathbf{x})|) = |\mu_g - \mu_{\widehat{g}}| \tag{43}$$

$$\begin{aligned} Var(\varepsilon) &= Var(|g(\mathbf{x}) - \widehat{g}(\mathbf{x})|) \\ &= Var(\text{sgn}(g(\mathbf{x}) - \widehat{g}(\mathbf{x}))(g(\mathbf{x}) - \widehat{g}(\mathbf{x}))) \\ &= (\text{sgn}(g(\mathbf{x}) - (\mathbf{x})))^2 Var(g(\mathbf{x})) + (-\text{sgn}(g(\mathbf{x}) - \widehat{g}(\mathbf{x})))^2 Var(\widehat{g}(\mathbf{x})) \\ &= \sigma_{\widehat{g}}^2 \end{aligned} \tag{44}$$

By substituting Eqs. (42)–(44) into Eq. (23) and ignoring the constraints, the OPF degrades into U function, which is depicted by

$$U = \frac{\left| \mu_{g(\mathbf{x})} - \mu_{\widehat{g}(\mathbf{x})} \right|}{\sigma_{\widehat{g}(\mathbf{x})}} \tag{45}$$

From the above analysis, it can be found that U function is acquired by constructing the accordingly optimization model, which verifies the feasibility and potential of OPM for solving different problems.

6. Examples

This section verifies the performance of the proposed OPM for both DO and RBDO problems, in which four DO and five RBDO prevalent active learning methods are compared, including method of moving asymptotes (MMA) [78], PoF [41], maximum MSE (MAX-MSE) [42], LCB [79], PMA [75,80], single loop approach (SLA) [81,82], LHS [83], U function [24,25], and expected risk function (ERF) [84]. All codes are implemented on a personal computer with configuration: Intel Core i9-13900K @3.0 GHz and 128 GB RAM.

6.1. A nonlinear example

The first example contains a nonlinear sin function [55,85], which has two random variables. The initial point is $[3,3]^{\text{T}}$. The SDs of both random variables are 0.1. Both DO and RBDO are considered, and their formulas are stated as Eqs. (46) and (47), respectively.

$$\begin{aligned} &\text{find } \mathbf{x} = [x_1, x_2]^{\text{T}} \\ &\min (x_1 - 3.7)^2 + (x_2 - 4)^2 \\ &\text{s.t.} g_j(\mathbf{x}) < 0 \, j = 1, 2 \\ &0 \le x_1 \le 3.7, 0 \le x_2 \le 4 \\ &\text{where } g_1(\mathbf{x}) = -x_1 \sin(4x_1) - 1.1x_2 \sin(2x_2) \\ &g_2(\mathbf{x}) = x_1 + x_2 - 3 \end{aligned} \tag{46}$$
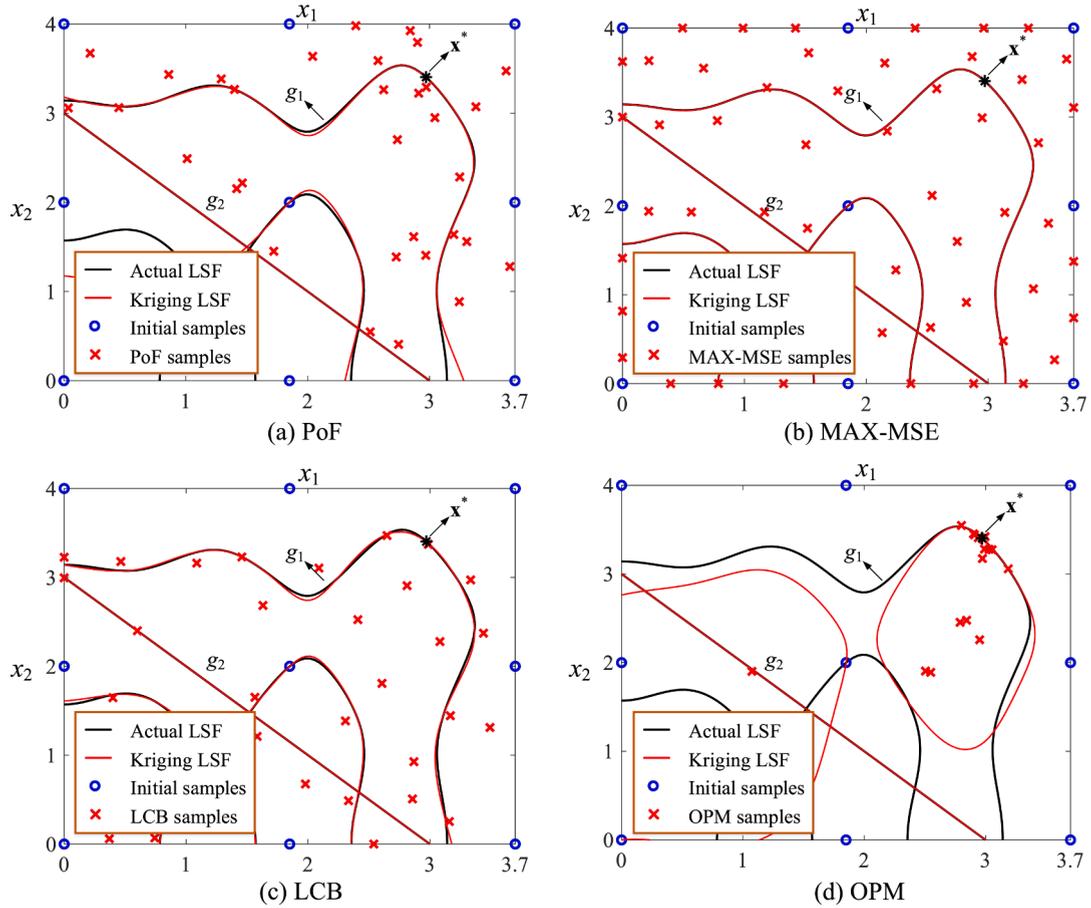
Fig. 2. Different DO methods of example 1 (a) PoF (b) MAX-MSE (c) LCB (d) OPM.

$$\text{find } \mathbf{d} = \left[\mu_{x_1}, \mu_{x_2} \right]^{\mathrm{T}}$$

$$\min \left(\mu_{x_1} - 3.7 \right)^2 + \left(\mu_{x_2} - 4 \right)^2$$

$$\text{s.t.Prob} \left[g_j(\mathbf{x}) < 0 \right] \leq \Phi \left(-\beta^t \right) j = 1, 2$$

$$0 \leq \mu_{x_1} \leq 3.7, 0 \leq \mu_{x_2} \leq 4 \tag{47}$$

$$\text{where } g_1(\mathbf{x}) = -x_1 \sin(4x_1) - 1.1x_2 \sin(2x_2)$$

$$g_2(\mathbf{x}) = x_1 + x_2 - 3$$

$$\beta_1^t = \beta_2^t = 2.0$$

The computational solutions are tabulated in Table 3. "F-evaluations" represents the number of function evaluations, while "Error" denotes the maximum relative error between Kriging models and real response functions (objective and performance functions) at the optimum. Since the MMA, PMA, and SLA are carried out based on the real objective and performance functions, the error is 0. Other methods, including PoF, MAX-MSE, LCB, LHS, U, ERF, and OPM, are performed based on Kriging model. 3-level full factorial design of the grid sampling is applied for these methods, in which nine initial points are generated, as shown in Fig. 2.

The diagrams of DO and RBDO are illustrated in Figs. 2 and 3, respectively. From Table 3, Fig. 2 and Fig. 3, it can be seen that MAX-MSE only uses the information of the predicted variance, and thus the samples are uniformly generated in the design space. For PoF, some samples are distributed around the LSF. Compared to the PoF and MAX-MSE, the samples of LCB are uniformly distributed in the vicinity of LSF. Therefore, the LSF predicted by the PoF and LCB is very close to the real LSF. However, the OPM can capture the importance domain in the design space, so the efficiency is significantly improved. The required samples of OPM are only about half of those of PoF and LCB. Also, the computational accuracy of OPM is promoted. For RBDO, PMA and SLA find the same optimum. Similar as MAX-MSE, samples generated by the LHS uniformly cover the design space. However, the error of LHS is up to 0.6844, which cannot be accepted. This is because that RBDO should ensure the global and local accuracies, which is more complex than DO problem. LHS, U, and ERF methods generate the samples on the LSF, and thus the accuracy of computing LSF is greatly promoted. Comparing with other methods, the OPM constructs the active leaning function from the viewpoint of the optimization theory, in which the objective
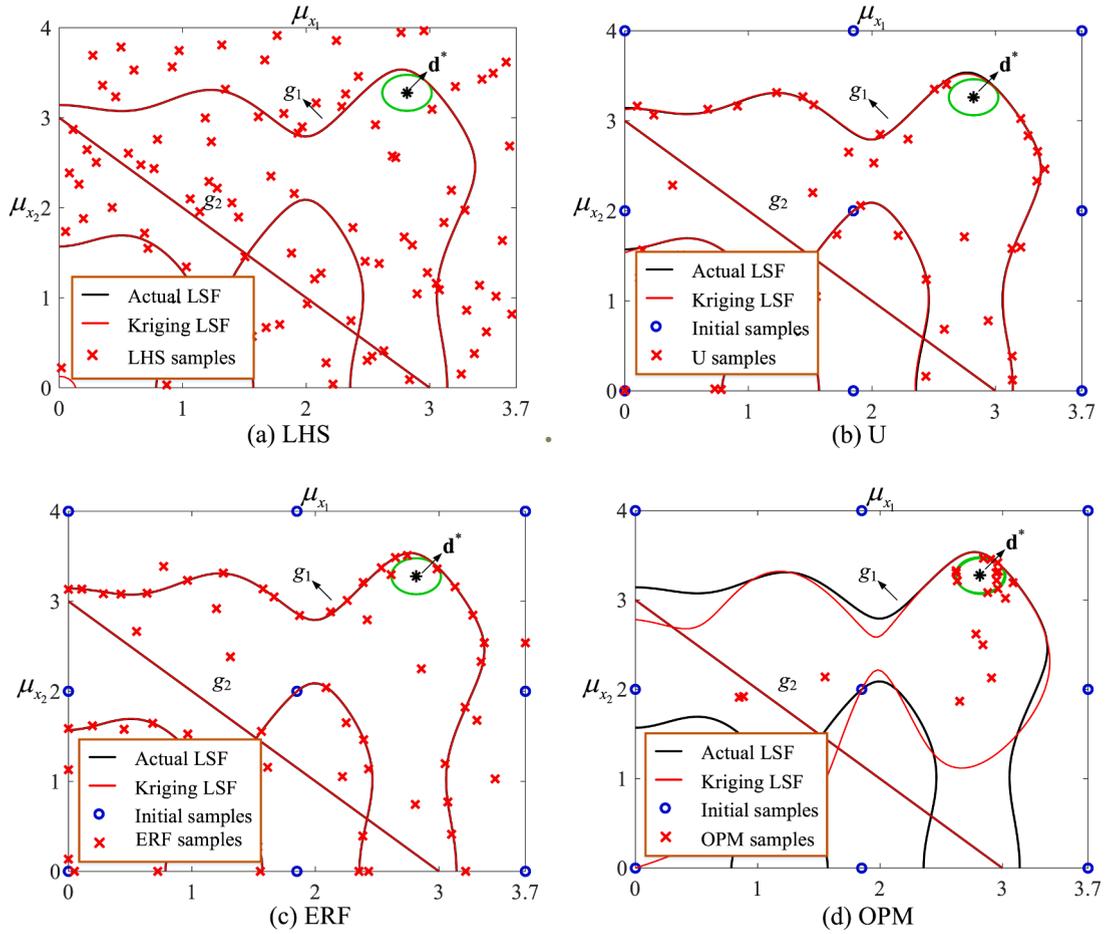
Fig. 3. Different RBDO methods of example 1 (a) LHS (b) MAX-MSE (c) LCB (d) OPM.

and performance functions are simultaneously considered. Therefore, the samples generated by OPM in the first stage locate in the local importance region, thereby reducing the sample number to a great extent. Then, the RBDO is performed to obtain the approximate optimum. In the second stage, the samples are generated on the target reliability surface, and the local accuracy is further improved. In general, OPM can adaptively identify the local importance region for solving both DO and RBDO problems, thereby narrowing the design space to a great extent. Thus, it exhibits the superiority in terms of efficiency and accuracy.

6.2. A multiple constraint example

The second example is a benchmark example that is widely used for comparison [86,87]. The initial point is $[5,5]^T$, and the SDs of both random variables are 0.3. Both DO and RBDO cases are tested, and their formulas are stated as Eqs. (48) and (49), respectively.

$$
\begin{aligned}
&\text{find } \mathbf{x} = [x_1, x_2]^T \\
&\min x_1 + x_2 \\
&\text{s.t.} g_j(\mathbf{x}) \le 0, j = 1, 2, 3 \\
&0 \le x_1 \le 10, 0 \le x_2 \le 10 \\
&\text{where } g_1(\mathbf{x}) = 1 - \frac{x_1^2 x_2}{20} \\
&g_2(\mathbf{x}) = 1 - \frac{(x_1 + x_2 - 5)^2}{30} - \frac{(x_1 - x_2 - 12)^2}{120} \\
&g_3(\mathbf{x}) = 1 - \frac{80}{(x_1^2 + 8x_2 + 5)}
\end{aligned}
\tag{48}
$$

Table 4
Results for example 2.

Methods	Objective	Design variables	F-evaluations	Error
DO				
MMA	5.1765	(3.1139,2.0626)	150	—
PoF	5.1836	(3.1176,2.0659)	32	3.0943×10^{-3}
MAX-MSE	5.1788	(3.1151,2.0637)	44	1.1036×10^{-4}
LCB	5.1735	(3.1123,2.0612)	37	1.3941×10^{-4}
OPM	5.1766	(3.1139,2.0627)	20	4.9301×10^{-5}
RBDO				
PMA	6.7257	(3.4391,3.2866)	969	—
SORA	6.7257	(3.4391,3.2866)	258	—
LHS	6.7236	(3.4376,3.2860)	50	2.0398×10^{-2}
U	6.7256	(3.4391,3.2866)	49	9.8341×10^{-6}
ERF	6.7256	(3.4390,3.2866)	60	7.2734×10^{-4}
OPM	6.7257	(3.4391,3.2866)	24	1.6254×10^{-5}
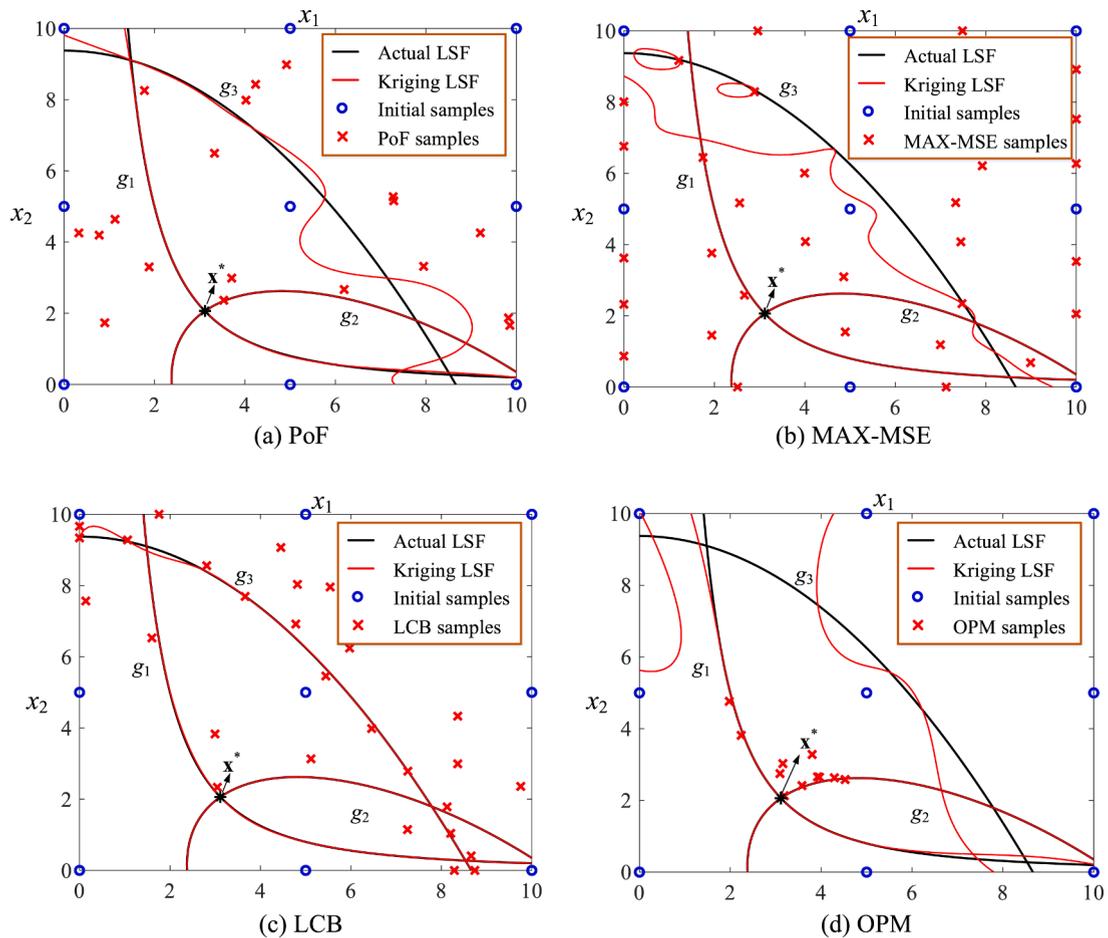
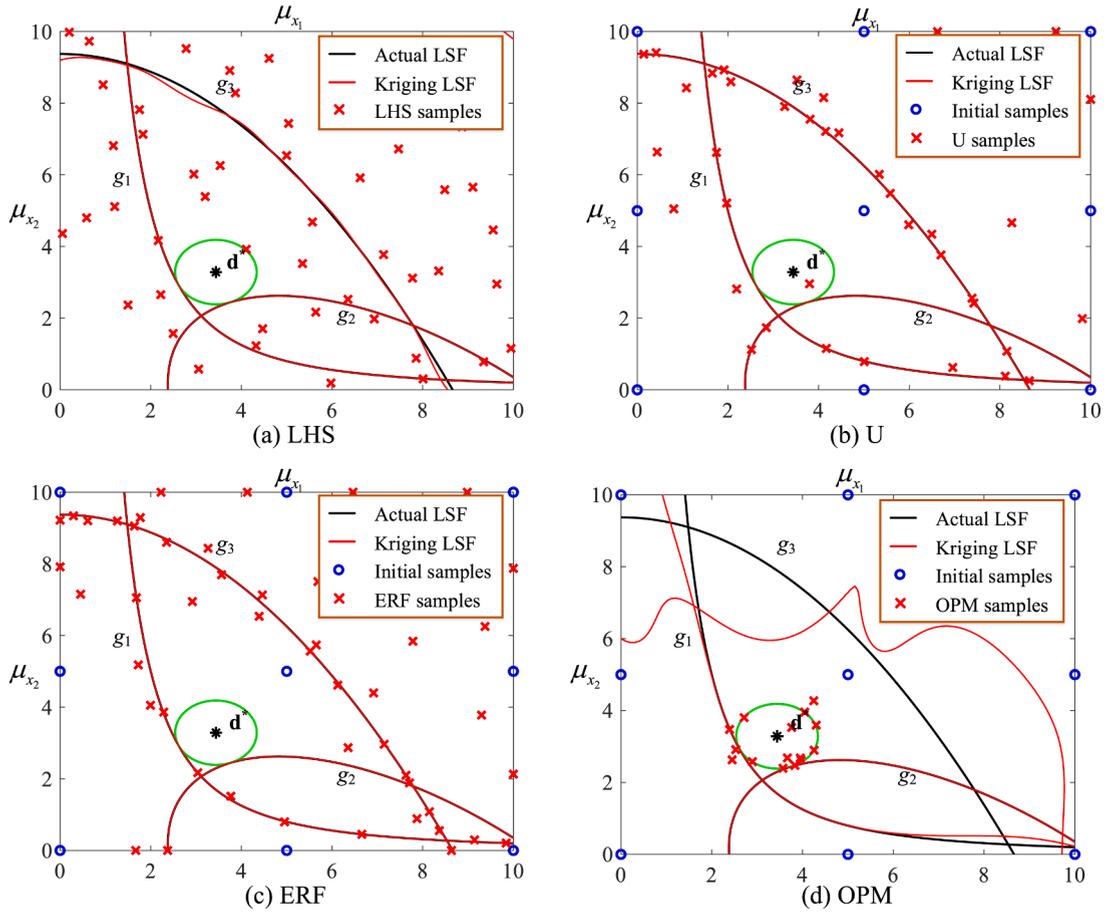**Fig. 4.** Different DO methods of example 2 (a) Pof (b) MAX-MSE (c) LCB (d) OPM.

Fig. 5. Different RBDO methods of example 2 (a) LHS (b) MAX-MSE (c) LCB (d) OPM.

$$\text{find } \mathbf{d} = \left[\mu_{x_1}, \mu_{x_2}\right]^{\mathrm{T}}$$

$$\min \mu_{x_1} + \mu_{x_2}$$

$$\text{s.t.} \text{Prob}\left[g_j(\mathbf{x}) < 0\right] \leq \Phi(-\beta^t), j = 1,2,3$$

$$0 \leq \mu_{x_1} \leq 10, 0 \leq \mu_{x_2} \leq 10$$

$$\text{where } g_1(\mathbf{x}) = 1 - \frac{x_1^2 x_2}{20} \tag{49}$$

$$g_2(\mathbf{x}) = 1 - \frac{(x_1 + x_2 - 5)^2}{30} - \frac{(x_1 - x_2 - 12)^2}{120}$$

$$g_3(\mathbf{x}) = 1 - \frac{80}{(x_1^2 + 8x_2 + 5)}$$

$$\beta_1^t = \beta_2^t = \beta_3^t = 3.0$$

The comparison results are summarized in Tables 4. 3-level full factorial design of the grid sampling is used, in which nine initial points are generated for all DO and RBDO methods. The diagrams of DO and RBDO are illustrated in Figs. 4 and 5, respectively. MMA, PMA, and SORA use the actual objective and performance functions, and thus they are used as the reference solutions. It can be seen that PMA and SORA find the same optimum.

For this benchmark example, since the nonlinearity of LSF is low, the computational error of all Kriging methods, i.e. PoF, MAX-MSE, LCB, LHS, U, and ERF, are acceptable. For DO, PoF and LCB are more efficient than MAX-MAE by using the information of predicted values and variance, while the computational cost of OPM is nearly 2-3 times less than those of the above-mentioned methods. For RBDO method, the accuracy of LHS is the worst. Compared to the LHS, the samples generated by U and ERF are located around the LSFs, so the accuracy is significantly promoted. In general, traditional methods can achieve a good global approximation, which leads to generating a large number of samples. However, OPM focuses on finding a good local approximation in the vicinity of optimum. Therefore, OPM is the most efficient and accurate method. Although the nonlinearity of this example is very
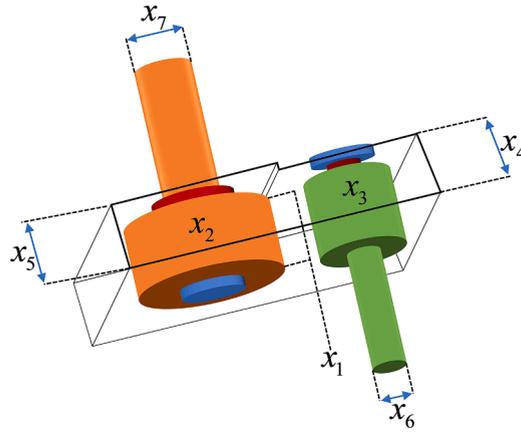
Fig. 6. A speed reducer.

low, the efficiency is still significantly improved. For both DO and RBDO problems, the computational cost of OPM is at least 2 times less than other methods.
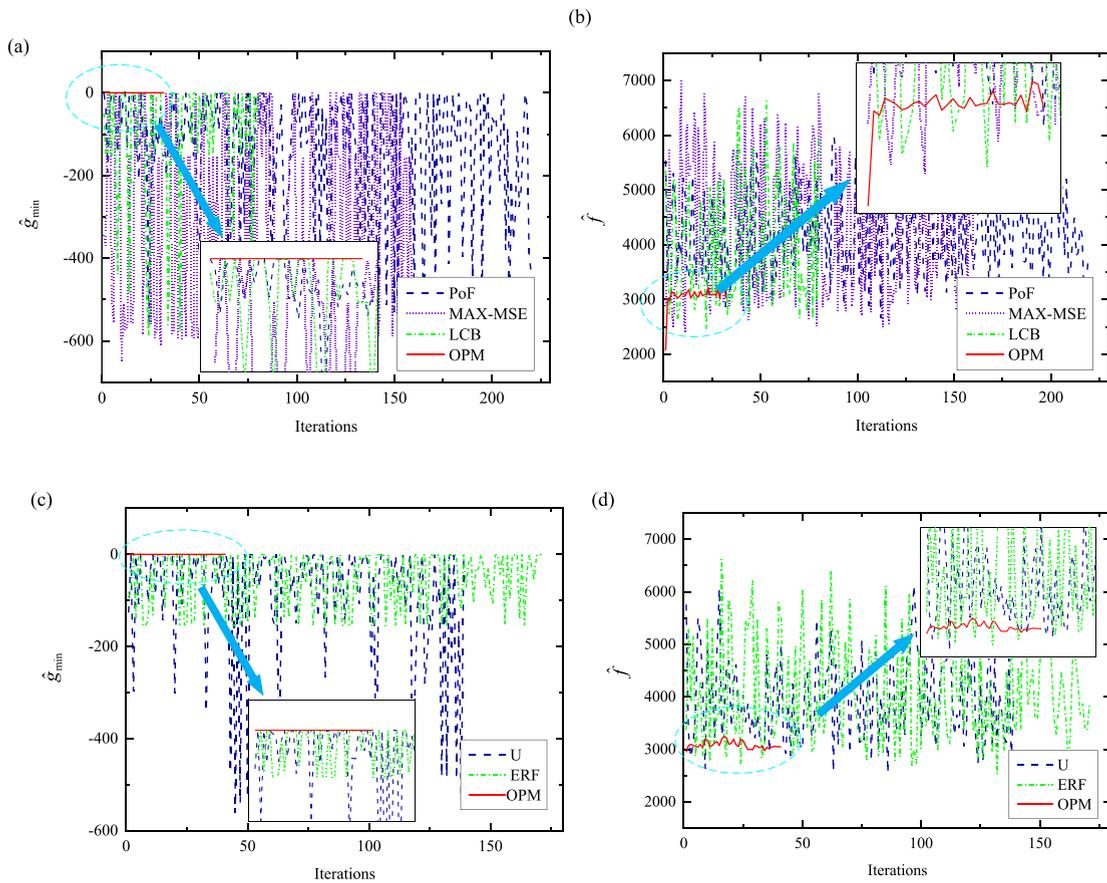
6.3. A speed reducer

The lightweight design of the speed reducer is performed in Fig. 6, which involves 7 random variables and 11 constraints [76]. The midpoint of design variables is used as the initial point. The SDs of all random variables are 0.005. Also, both DO and RBDO cases are tested, and their formulas are stated as Eqs. (50) and (51), respectively.

$$
\begin{aligned}
&\text{find } \mathbf{x} = [x_1, x_2, x_3, x_4, x_5, x_6, x_7]^{\mathrm{T}} \\
&\min f(\mathbf{x}) = 0.7854 x_1 x_1^2 \left(3.3333 x_3^2 + 14.9334 x_3 - 43.0934\right) \\
&\qquad -1.508 x_1 \left(x_6^2 + x_7^2\right) + 7.477 \left(x_6^3 + x_7^3\right) + 0.7854 \left(x_4 x_6^2 + x_5 x_7^2\right) \\
&\text{s.t.} g_j(\mathbf{x}) \leq 0, \quad j = 1, \ldots, 11 \\
&g_1(\mathbf{x}) = -\frac{27}{x_1 x_2^2 x_3} + 1, g_2(\mathbf{x}) = -\frac{397.5}{x_1 x_2^2 x_3^2} + 1, \\
&g_3(\mathbf{x}) = -\frac{1.93 x_4^3}{x_2 x_3 x_6^4} + 1, g_4(\mathbf{x}) = -\frac{1.93 x_5^3}{x_2 x_3 x_7^4} + 1, \\
&g_5(\mathbf{x}) = -\frac{\sqrt{\left(745 x_4/(x_2 x_3)\right)^2 + 16.9 \times 10^6}}{0.1 x_6^3} + 1100, \\
&g_6(\mathbf{x}) = -\frac{\sqrt{\left(745 x_5/(x_2 x_3)\right)^2 + 157.5 \times 10^6}}{0.1 x_7^3} + 850, \\
&g_7(\mathbf{x}) = -x_2 x_3 + 40, g_8(\mathbf{x}) = -5 + \frac{x_1}{x_2}, \\
&g_9(\mathbf{x}) = -\frac{x_1}{x_2} + 12, g_{10}(\mathbf{x}) = -\frac{1.5 x_6 + 1.9}{x_4} + 1, \\
&g_{11}(\mathbf{x}) = -\frac{1.1 x_7 + 1.9}{x_5} + 1 \\
&2.6 \leq x_1 \leq 3.6, \ 0.7 \leq x_2 \leq 0.8, 17 \leq x_3 \leq 28 \\
&7.3 \leq x_4 \leq 8.3, \ \ 7.3 \leq x_5 \leq 8.3 \\
&2.9 \leq x_6 \leq 3.9, \ 5.0 \leq x_7 \leq 5.5
\end{aligned}
\tag{50}
$$

Table 5
Results for example 3.

Methods	Objective	Design variables	F-evaluations	Error
DO				
MMA	2994.34	(3.5000,0.7,17.0,7.3,7.7153,3.3502,5.2867)	1112	—
PoF	2989.98	(3.5004,0.7,17.0,7.3,7.7157,3.3502,5.2866)	256	0.0168
MAX-MSE	2997.22	(3.5001,0.7,17.0,7.3,7.7156,3.3522,5.2868)	196	0.0151
LCB	2995.59	(3.5009,0.7,17.0,7.3,7.7151,3.3502,5.2866)	116	0.0074
OPM	2994.62	(3.5001,0.7,17.0,7.3,7.7156,3.3496,5.2869)	68	0.0020
RBDO				
PMA	3038.61	(3.5765,0.7,17.0,7.3,7.7541,3.3652,5.3017)	1240	—
SORA	3038.61	(3.5765,0.7,17.0,7.3,7.7541,3.3652,5.3017)	648	—
LHS	3035.44	(3.5671,0.7,17.0,7.3,7.7540,3.3675,5.3015)	300	0.0138
U	3010.47	(3.5771,0.7,17.0,7.3,7.7541,3.3658,5.3016)	175	0.0079
ERF	3038.08	(3.5762,0.7,17.0,7.3,7.7543,3.3650,5.3014)	207	0.0061
OPM	3038.53	(3.5764,0.7,17.0,7.3,7.7541,3.3652,5.3016)	77	1.8213×10^{-5}

Fig. 7. Iterative histories of different methods for the speed reducer (a) constraint with the minimum value for DO methods (b) objective for DO methods (c) constraint with the minimum value for RBDO methods (d) objective for RBDO methods.
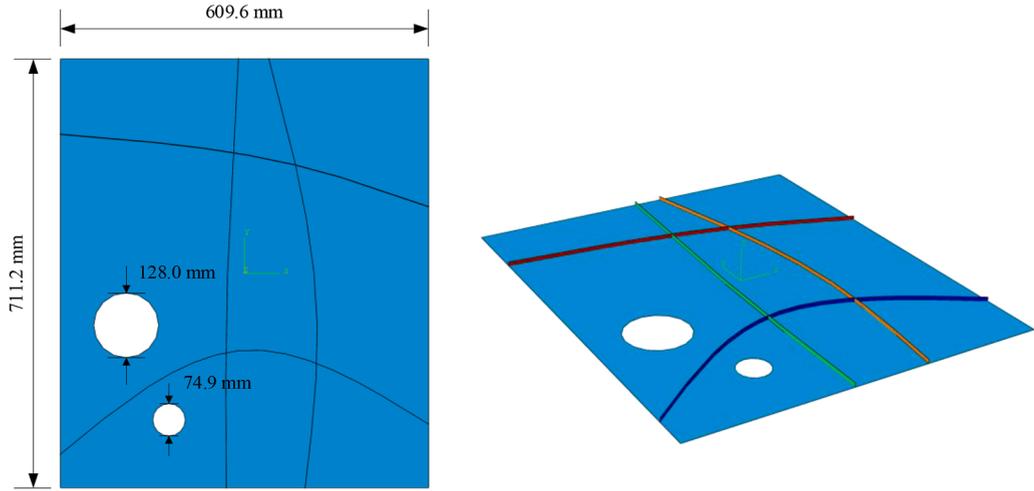
Fig. 8. Stiffened plate with cutouts.

find $\mathbf{x} = \left[\mu_{x_1}, \mu_{x_2}, \mu_{x_3}, \mu_{x_4}, \mu_{x_5}, \mu_{x_6}, \mu_{x_7} \right]^{\mathrm{T}}$

$\min f(\mathbf{x}) = 0.7854 \mu_{x_1}^2 \left(3.3333 \mu_{x_3}^2 + 14.9334 \mu_{x_3} - 43.0934 \right)$

$\qquad - 1.508 \mu_{x_1} \left(\mu_{x_6}^2 + \mu_{x_7}^2 \right) + 7.477 \left(\mu_{x_6}^3 + \mu_{x_7}^3 \right) + 0.7854 \left(\mu_{x_4} \mu_{x_6}^2 + \mu_{x_5} \mu_{x_7}^2 \right)$

$\mathrm{s.t.} \operatorname{Prob} \left[g_j(\mathbf{x}) < 0 \right] \leq \Phi(-\beta^t), j = 1, \ldots, 11$

$g_1(\mathbf{x}) = -\dfrac{27}{x_1 x_2^2 x_3} + 1, g_2(\mathbf{x}) = -\dfrac{397.5}{x_1 x_2^2 x_3^2} + 1,$

$g_3(\mathbf{x}) = -\dfrac{1.93 x_4^3}{x_2 x_3 x_6^4} + 1, g_4(\mathbf{x}) = -\dfrac{1.93 x_5^3}{x_2 x_3 x_7^4} + 1,$

$g_5(\mathbf{x}) = -\dfrac{\sqrt{\left(745 x_4/(x_2 x_3)\right)^2 + 16.9 \times 10^6}}{0.1 x_6^3} + 1100,$

$g_6(\mathbf{x}) = -\dfrac{\sqrt{\left(745 x_5/(x_2 x_3)\right)^2 + 157.5 \times 10^6}}{0.1 x_7^3} + 850,$ $\qquad(51)$

$g_7(\mathbf{x}) = -x_2 x_3 + 40, g_8(\mathbf{x}) = -5 + \dfrac{x_1}{x_2},$

$g_9(\mathbf{x}) = -\dfrac{x_1}{x_2} + 12, g_{10}(\mathbf{x}) = -\dfrac{1.5 x_6 + 1.9}{x_4} + 1,$

$g_{11}(\mathbf{x}) = -\dfrac{1.1 x_7 + 1.9}{x_5} + 1$

$2.6 \leq x_1 \leq 3.6, \ 0.7 \leq x_2 \leq 0.8, 17 \leq x_3 \leq 28$

$7.3 \leq x_4 \leq 8.3, \ \ 7.3 \leq x_5 \leq 8.3$

$2.9 \leq x_6 \leq 3.9, \ 5.0 \leq x_7 \leq 5.5$

Table 5 summarizes the results. The LHS method is used to generate the initial points, in which 36 points are used for all DO and RBDO methods. MMA, PMA, and SORA use the actual objective and performance functions, and thus they are used as the reference solutions. It can be seen that PMA and SORA find the same optimum.

Since this example contains multiple variables and constraints, the design space is large and the response is complex. Therefore, more samples are required to promote the accuracy. From Table 5, it can be seen that PoF and MAX-MSE exhibit some errors, and the computational efficiency is low. The samples of LCB are only about half of those of PoF and MAX-MSE. For RBDO, it is more complicate than DO, thus it requires more samples. LHS also shows some errors, while the efficiency and accuracy of U and ERF methods are significantly promoted. For DO, the OPM is 1.7059, 2.8824, and 3.7647 times faster than LCB, MAX-MSE, and PoF, respectively. For RBDO, the OPM is 2.6883 and 2.2727 times faster than U and ERF, respectively. The iterative histories of both DO and RBDO methods are illustrated in the Fig. 7. It can be observed that OPM quickly finds the important region, and the generated samples are clustered in this local region around the LSF. In general, the efficiency of OPM is significantly promoted.

Table 6
Results for example 4.

| Methods	Objective	Design variables	F-evaluations	Error
DO				
MMA	2.9828	(2.3394,17.6478,1.6024)	96	—
PoF	2.4859	(1.8219,18.0000,2.4400)	54	0.1974
MAX-MSE	2.9453	(2.3285,18.0000,1.3839)	227	0.0077
LCB	2.9673	(2.3422,18.0000,1.4347)	172	0.0021
OPM	2.9644	(2.3099,18.0000,1.6899)	53	0.0081
RBDO				
PMA	3.4775	(2.7434,17.7222,1.7211)	6162	—
LHS	3.4693	(2.6798,18.0000,2.1787)	300	0.0104
U	3.4681	(2.7305,18.0000,1.7369)	60	0.0476
ERF	3.4834	(2.7230,17.8172,1.9303)	117	0.0516
OPM	3.4301	(2.6605,18.0000,2.0607)	46	5.1241×10^{-4}
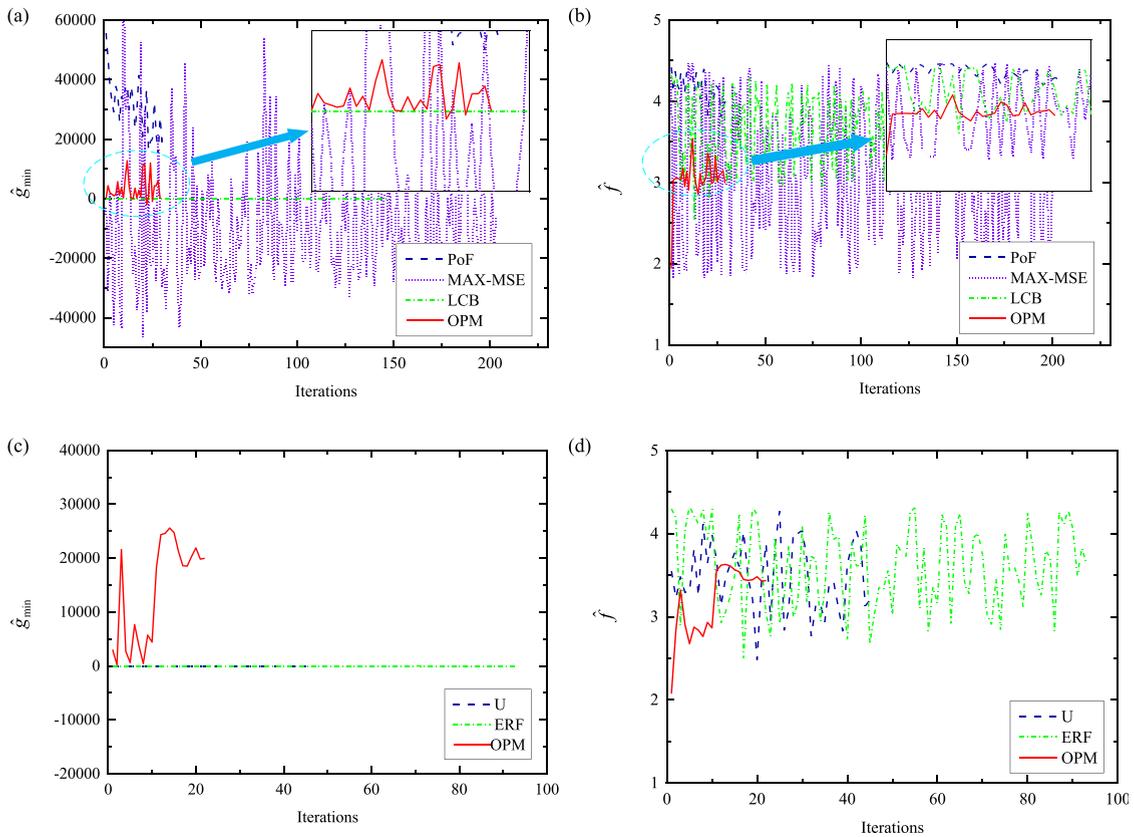
Fig. 9. Iterative histories of different methods for the stiffened plate (a) constraint with the minimum value for DO methods (b) objective for DO methods (c) constraint with the minimum value for RBDO methods (d) objective for RBDO methods.

6.4. A stiffened plate with cutouts

The stiffened plate is widely used in aerospace engineering [88]. Owing to performance requirement, it always exists cutouts. In this case, a curvilinear stiffened plate is tested, in which skin thickness t_s, stiffer height h, and stiffer width t are design and random variables, as shown in Fig. 8. Besides, the elasticity modulus E and Poisson ratio ν are regarded as random variables. Their means and SDs of $[t_s, t, h, E, \nu]$ are [2.6 mm,13.4 mm,1.6 mm,70 GPa, 0.33] and [0.13, 0.67, 0.08, 3.5, 0.0165], and the means of geometric dimension are considered as initial point. Its weight is minimized, and the buckling load capacity P_{cr} of the stiffened plate should be larger than the allowable value. The DO and RBDO are tested, and their formulas are stated as Eqs. (52) and (53), respectively.
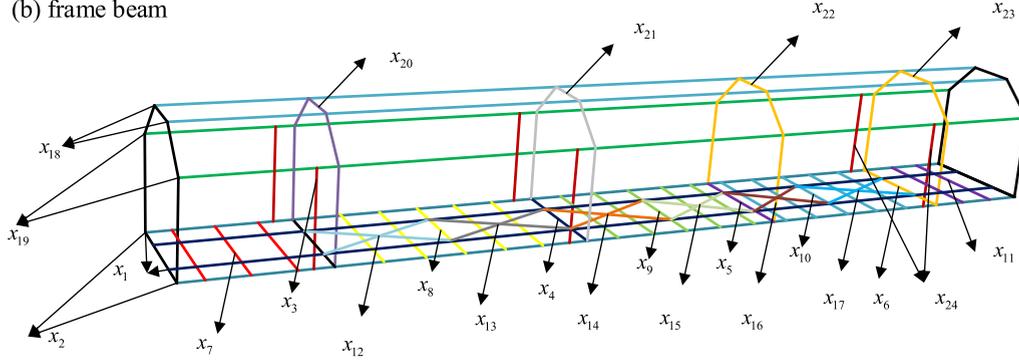
(a) corrugated plate
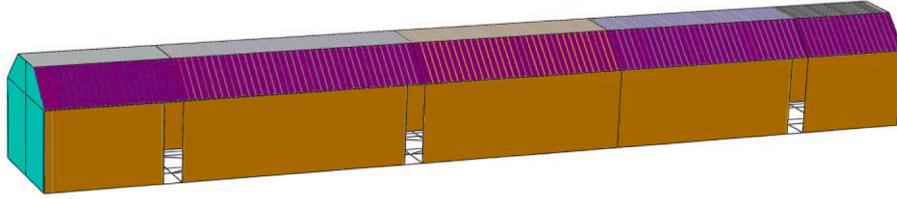
(b) frame beam

Fig. 10. A carriage structure (a) corrugated plate (b) frame beam.

Table 7
Design variables of the carriage structure.

Variables	x_1 (mm)	x_2 (mm)	$x_3 \sim x_6$ (mm)	$x_7 \sim x_{18}$ (mm)	$x_{19} \sim x_{23}$ (mm)	x_{24} (mm)
Initial	6	4	8	4	5	4
Lower	4	2.5	5	2.5	3.3	2.5
Upper	8	5.5	11	5.5	6.6	5.5

$$
\begin{aligned}
&\text{find } [t_s, t, h]^T \\
&\text{min Weight} \\
&\text{s.t.} g(t_s, t, h, E, \nu) \leq 0 \\
&g = 39455\text{N} - P_{cr} \\
&1.5 \leq t_s \leq 3.5, 0.8 \leq t \leq 2.4, 8.0 \leq h \leq 18.0
\end{aligned}
\tag{52}
$$

$$
\begin{aligned}
&\text{find } [t_s, t, h]^T \\
&\text{minWeight} \\
&\text{s.t.Prob}[g(t_s, t, h, E, \nu) < 0] \leq \Phi(-\beta^t) \\
&g = 39455\text{N} - P_{cr} \\
&1.5 \leq t_s \leq 3.5, 0.8 \leq t \leq 2.4, 8.0 \leq h \leq 18.0
\end{aligned}
\tag{53}
$$

Table 6 summarizes the results. The initial points are generated by the LHS method, in which 24 points are used for all DO and RBDO methods. MMA and PMA use the actual objective and performance functions, and they are used as the reference solutions.

For this complex engineering example, it has multiple optima [88], thus MMA and OPM find the different optimum, as well as PMA and OPM. For buckling response, the nonlinearity of LSF is high, and thus it is hard to predict the LSF in the whole design space. Therefore, PoF, MAX-MSE, and LCB require many samples to ensure the accuracy. The computational cost of U and ERF is reduced through adding the samples on the LSFs. However, the predicted accuracy is low. OPM exhibits the superiority over other methods. The iterative histories of both DO and RBDO methods are illustrated in the Fig. 9. The OPM can identify the importance region adaptively, and the samples generated by OPM are clustered in this region. For RBDO, the performance function amplitude is large, thus the generated samples in the second stage have some distances from the LSF, as plotted in Figs. 9 (c) and (d). In general, the utilization ratio of samples is promoted, and the efficiency and accuracy are significantly promoted by using the OPM.

6.5. A high-dimensional carriage structure

In this section, the DO and RBDO problems of the carriage structure is studied to validate the applicability of the proposed OPM in

Table 8
Results for the carriage structure.

Methods	Objective	Design variables	F-evaluations	Error
DO				
PoF	86.7864	(4.0000,3.6733,5.0023,5.0002,5.0001,7.0161, 4.5008,5.5000,2.5001,2.5003,2.5006,3.5143, 2.5002,2.5000,2.5000,2.7172,2.9991,2.5000, 3.3000,3.3000,3.3000,3.0009,3.3005,2.6053)	718	0.3459
MAX-MSE	88.8197	(4.0000,5.0766,7.7910,5.0085,5.0334,10.9988, 3.1252,4.4343,2.5025,5.5000,3.1981,3.4519, 3.7731,2.5004,2.5000,2.5015,2.5000,2.5130, 3.3000,3.3000,3.0008,3.3004,6.6000,2.5001)	1050	0.0325
LCB	88.3243	(4.0001,4.9121,6.1159,5.0034,7.3885, 5.5000,2.5010,4.1290,5.4997,2.5005,4.5245, 2.5037,2.5015,5.4996,2.5199,4.4040,2.5002, 3.3186,3.3012,3.3000,3.3000,4.6485,2.5000)	1050	0.0410
OPM	88.6204	(4.0028,4.7840,7.3066,7.3212,5.0730,8.7099, 5.1104,4.4303,2.5000,5.4936,2.5009,2.5003, 2.5000,2.6294,2.5351,5.5000,2.5001,2.5000, 3.3000,3.3000,3.3003,3.3222,6.6000,2.5135)	479	0.0221
RBDO				
U	86.5534	(4.0000,3.5695,5.0000,5.0564,5.0000,5.0001, 2.5231,2.5132,2.5001,3.4714,4.0654,2.5037, 4.4497,5.1839,2.5087,2.5015,4.3094,2.5002, 3.3000,3.3000,3.3086,3.3000,3.3002,2.5099)	693	0.8114
ERF	87.5955	(4.0000,4.3457,5.0001,5.0003,6.0388,5.0913, 3.2177,2.5000,2.5000,5.5000,5.4058,2.5000, 3.4291,2.9698,5.5000,2.5277,3.3630,2.5000, 3.3011,3.3000,3.3000,4.3799,4.5733,2.5000)	486	0.4361
OPM	89.7026	(4.0000,4.1648,10.5611,9.3668,8.5170,5.0000, 5.1547,2.5011,4.3437,5.4998,2.5000,5.5000, 3.4266,3.2088,5.4986,3.5445,3.7976,4.4507, 3.3002,4.0631,3.3147,3.3135,6.5994,2.5000)	417	0.0482

engineering application, and it is composed by the corrugated plate and frame beam. The geometric size is 47 m × 6.5 m × 4.63 m. The carriage profile is plotted in Fig. 10. The carriage is subject to inertial forces generated by its own gravity and acceleration, where the gravitational acceleration and the forward acceleration of the carriage are 9.8 m^2/s. Its weight is minimized. The maximum displacement U_1 should be less than the allowable value of 14.2 mm. It contains 24 design variables, which are illustrated in Fig. 10 (b). Table 7 lists the initial design, upper bound, and lower bound. For RBDO, they also are deemed as the random variables with coefficient of variation 0.05. The door of this carriage structure is composed by the aluminum. The density is 2.7 × 10^{-6} kg/mm^3, and the elasticity modulus is 70 GPa. The rest of the carriage is made by steel. The elasticity modulus and Poisson ratio are 210 GPa and 0.3, respectively. The DO and RBDO models are expressed by Eqs. (54) and (55), respectively.

$$\begin{aligned}
&\text{find } [x_1, x_2, ..., x_{24}]^T \\
&\min \text{Weight} \\
&\text{s.t. } U_1 - 14.2\,\text{mm} \le 0
\end{aligned} \tag{54}$$

$$\begin{aligned}
&\text{find } [x_1, x_2, ..., x_{24}]^T \\
&\min \text{Weight} \\
&\text{s.t. Prob}[U_1 - 14.2\,\text{mm} \le 0] \le \Phi(-\beta^t) \\
&\beta^t = 3
\end{aligned} \tag{55}$$

Table 8 summarizes the results. The LHS is adopted to generate the initial samples, in which 50 initial points are used. Since this engineering example contains high-dimensional design and random variables, it confronts the great challenge. The maximum sample number generated by the learning method is 1000.

MMA and PMA appear oscillation and are difficult to find the optimum. Other results are Table 8. The results obtained by OPM at the optimum are illustrated in Fig. 11. For DO, the accuracy of Pof is low. MAX-MSE and LCB improve the computational accuracy, but their sample sizes are large. OPM outperforms other active learning methods in terms of accuracy and efficiency. For RBDO, since it needs ensuring the computational accuracy of the reliability analysis, it is more complex than DO problem. In this situation, the U and ERF functions meet the inaccurate problem, and their errors are up to 81.14 and 43.61 %. The accuracy cannot be accepted. OPM is far more efficient and accurate than other methods, and the error is only 4.82 %. It can be concluded that OPM exhibits the highest accuracy and efficiency for this high-dimensional engineering example.

7. Conclusions

In this paper, a new OPM based on the active learning technique of Kriging metamodel is proposed from the viewpoint of
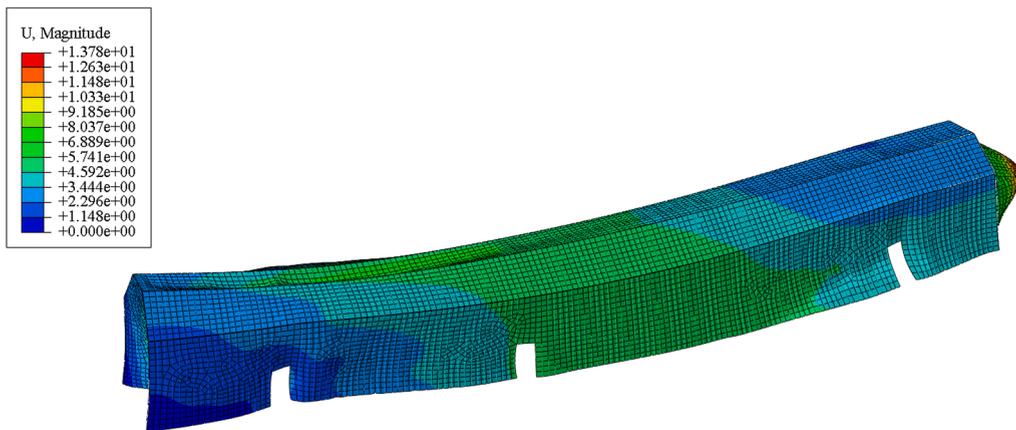
(a) DO
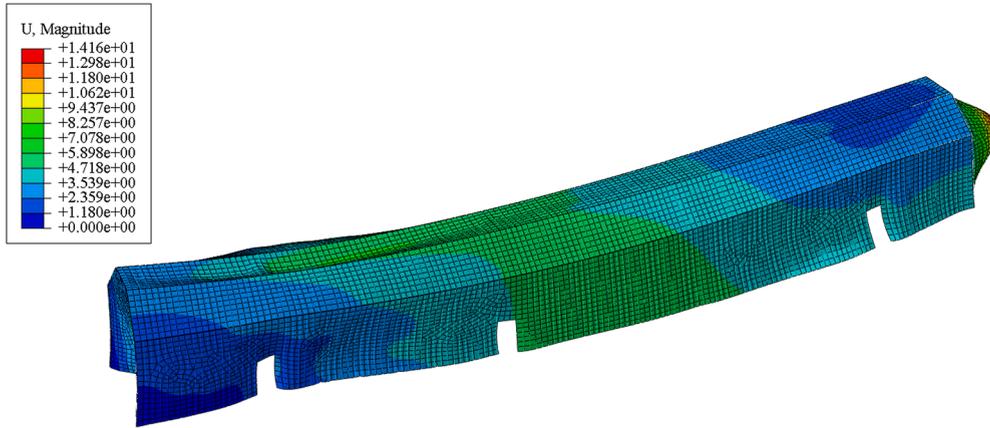
(b) RBDO

Fig. 11. Displacement of the carriage structure of OPM at the optimum (a) DO (b) RBDO.

optimization theory, in which the OPF and AOPF are constructed for DO and RBDO, respectively. Counter to the well-known active learning methods, OPM has a straightforward and easy implementation, according to its rigorous mathematical foundation, to circumstance this problem. Also, it proves the validity via deriving the typical U function. It not only provides the theoretical support for U function, but also validates the effectiveness and reasonability of OPM. In general, OPM can comprehensively consider the objective function, constraints, and their relationship. Moreover, the AOPM expedites convergence of the MPTP and the optimum of RBDO with enough accuracy.

Comprehensive tests are implemented to test the performance of the proposed OPM, in which two benchmark and three real-world engineering examples are employed. Different metrics, including the number of samples, objective, optimum, error, and the sample distribution, are applied to reflect the performance of the Kriging method, which aims to confirm the remarkable promotion of the proposed OPM for solving both mathematical and engineering examples. In general, we have proposed the OPM with a simple work, which only derives the active learning function by constructing the optimization formulation. From the results, it can be found that the traditional methods require a global approximation of the objective and constraint functions, which leads to significantly computational burden. In contrast, the proposed OPM enhances the efficiency by employing a local approximation around the optimum. In the future, we will continue to explore other optimization problems, e.g. multi-objective optimization, robust design optimization, non-probabilistic RBDO, fuzzy optimization, hybrid RBDO optimization problem, etc. In addition, other improved versions of OPM can be developed by combining different algorithms, such as state-of-the-art optimization algorithms and sampling technologies.

CRediT authorship contribution statement

Zeng Meng: Conceptualization. **Lin Kong:** Investigation. **Jiaxiang Yi:** Validation. **Hao Peng:** Methodology, Supervision.

Declaration of Competing Interest

The authors declare that they have no known competing financial interests or personal relationships that could have appeared to influence the work reported in this paper.

Data availability

Data will be made available on request.

Acknowledgments

Appendix

Assume that two Kriging models $\widehat{f}(x)$ and $\widehat{g}(x)$ are separately established for $f(x)$ and $g(x)$. They are respectively stated as

$$\widehat{f}(\mathbf{x}) = \mathbf{h}_f^T(\mathbf{x})\boldsymbol{\gamma}_f + v_f(\mathbf{x}) \tag{I}$$

$$\widehat{g}(\mathbf{x}) = \mathbf{h}_g^T(\mathbf{x})\boldsymbol{\gamma}_g + v_g(\mathbf{x}) \tag{II}$$

where the coefficients are consistent with those in Section 2.3. The unbiased predictors $\mu_{\widehat{f}(\mathbf{x}_0)}$ and $\mu_{\widehat{g}(\mathbf{x}_0)}$ of $\widehat{f}(x)$ and $\widehat{g}(x)$ on an arbitrary point x_0 are respectively evaluated by

$$\widehat{\mu}_{\widehat{f}(\mathbf{x}_0)} = \mathbf{h}_f^T(\mathbf{x}_0)\widehat{\boldsymbol{\gamma}}_f + \mathbf{r}_{0f}^T\mathbf{R}_f^{-1}\left(\mathbf{f} - \mathbf{H}_f\widehat{\boldsymbol{\gamma}}_f\right) \tag{III}$$

$$\widehat{\mu}_{\widehat{g}(\mathbf{x}_0)} = \mathbf{h}_g^T(\mathbf{x}_0)\widehat{\boldsymbol{\gamma}}_g + \mathbf{r}_{0g}^T\mathbf{R}_g^{-1}\left(\mathbf{g} - \mathbf{H}_g\widehat{\boldsymbol{\gamma}}_g\right) \tag{IV}$$

where the coefficients are computed by Eqs. (4)–(8). The covariance between $\widehat{f}(x)$ and $\widehat{g}(x)$ are evaluated as follows:

$$
\begin{aligned}
Cov(\widehat{f}(\mathbf{x}_0), \widehat{g}(\mathbf{x}_0)) \; &= \mu(\widehat{f}(\mathbf{x}_0) \cdot \widehat{g}(\mathbf{x}_0)) - \widehat{\mu}_{\widehat{f}(\mathbf{x}_0)} \cdot \widehat{\mu}_{\widehat{g}(\mathbf{x}_0)} \\
&= \mu\left(\left(\mathbf{h}_f^T(\mathbf{x}_0)\boldsymbol{\gamma}_f + v_f(\mathbf{x}_0)\right)\left(\mathbf{h}_g^T(\mathbf{x}_0)\boldsymbol{\gamma}_g + v_g(\mathbf{x}_0)\right)\right) \\
&\quad - \left(\mathbf{h}_f^T(\mathbf{x}_0)\widehat{\boldsymbol{\gamma}}_f + \mathbf{r}_{0f}^T\mathbf{R}_f^{-1}\left(\mathbf{f} - \mathbf{H}_f\widehat{\boldsymbol{\gamma}}_f\right)\right)\left(\mathbf{h}_g^T(\mathbf{x}_0)\widehat{\boldsymbol{\gamma}}_g + \mathbf{r}_{0g}^T\mathbf{R}_g^{-1}\left(\mathbf{g} - \mathbf{H}_g\widehat{\boldsymbol{\gamma}}_g\right)\right) \\
&= \mathbf{h}_f^T(\mathbf{x}_0)\boldsymbol{\gamma}_f\left(\mu\left(v_g(\mathbf{x}_0)\right) - \mathbf{r}_{0g}^T\mathbf{R}_g^{-1}\left(\mathbf{g} - \mathbf{H}_g\widehat{\boldsymbol{\gamma}}_g\right)\right) \\
&\quad + \mathbf{h}_g^T(\mathbf{x}_0)\boldsymbol{\gamma}_g\left(\mu\left(v_f(\mathbf{x}_0)\right) - \mathbf{r}_{0f}^T\mathbf{R}_f^{-1}\left(\mathbf{f} - \mathbf{H}_f\widehat{\boldsymbol{\gamma}}_f\right)\right) \\
&\quad + \mu\left(v_f(\mathbf{x}_0) \cdot v_g(\mathbf{x}_0)\right) - \mathbf{r}_{0f}^T\mathbf{R}_f^{-1}\left(\mathbf{f} - \mathbf{H}_f\widehat{\boldsymbol{\gamma}}_f\right)\mathbf{r}_{0g}^T\mathbf{R}_g^{-1}\left(\mathbf{g} - \mathbf{H}_g\widehat{\boldsymbol{\gamma}}_g\right)
\end{aligned} \tag{V}
$$

Based on Eqs. (4)–(9), $\mu(v_g(\mathbf{x}_0))$ and $\mu(v_f(\mathbf{x}_0))$ are evaluated by

$$\mu\left(v_g(\mathbf{x}_0)\right) = \mathbf{r}_{0g}^T\mathbf{R}_g^{-1}\left(\mathbf{g} - \mathbf{H}_g\widehat{\boldsymbol{\gamma}}_g\right) \tag{VI}$$

$$\mu\left(v_f(\mathbf{x}_0)\right) = \mathbf{r}_{0f}^T\mathbf{R}_f^{-1}\left(\mathbf{f} - \mathbf{H}_f\widehat{\boldsymbol{\gamma}}_f\right) \tag{VII}$$

Then, Eq. (V) can be simplified as

$$Cov(\widehat{f}(\mathbf{x}_0), \widehat{g}(\mathbf{x}_0)) \; = \mu\left(v_f(\mathbf{x}_0) \cdot v_g(\mathbf{x}_0)\right) - \mathbf{r}_{0f}^T\mathbf{R}_f^{-1}\left(\mathbf{f} - \mathbf{H}_f\widehat{\boldsymbol{\gamma}}_f\right)\mathbf{r}_{0g}^T\mathbf{R}_g^{-1}\left(\mathbf{g} - \mathbf{H}_g\widehat{\boldsymbol{\gamma}}_g\right) \tag{VIII}$$

Since the two Kriging models $\widehat{f}(x)$ and $\widehat{g}(x)$ are separately established, $v_f(\mathbf{x}_0)$ and $v_g(\mathbf{x}_0)$ are independent Gaussian processes. Therefore, we have

$$
\begin{aligned}
\mu\left(v_f(\mathbf{x}_0) \cdot v_g(\mathbf{x}_0)\right) &= \mu\left(v_f(\mathbf{x}_0)\right) \cdot \mu\left(v_g(\mathbf{x}_0)\right) \\
&= \mathbf{r}_{0f}^T\mathbf{R}_f^{-1}\left(\mathbf{f} - \mathbf{H}_f\widehat{\boldsymbol{\gamma}}_f\right)\mathbf{r}_{0g}^T\mathbf{R}_g^{-1}\left(\mathbf{g} - \mathbf{H}_g\widehat{\boldsymbol{\gamma}}_g\right)
\end{aligned} \tag{IX}
$$

By combining Eqs. (VIII) and (IX), the covariance is obtained as follows:

$$Cov(\widehat{f}(\mathbf{x}_0), \widehat{g}(\mathbf{x}_0)) \; = 0 \tag{X}$$

Consequently, $\widehat{f}(x)$ and $\widehat{g}(x)$ are mutually independent. Similarly, the covariances between other separately established Kriging models are also **0**.

References

[1] X. Cai, L. Gao, X. Li, Efficient generalized surrogate-assisted evolutionary algorithm for high-dimensional expensive problems, IEEE Trans. Evol. Comput. 24 (2020) 365–379.

[2] N.D. Lagaros, V. Plevris, N.A. Kallioras, The Mosaic of metaheuristic algorithms in structural optimization, Arch. Comput. Meth. Eng. 29 (2022) 5457–5492.

[3] S. Mukherjee, D. Lu, B. Raghavan, P. Breitkopf, S. Dutta, M. Xiao, W. Zhang, Accelerating large-scale topology optimization: state-of-the-art and challenges, Arch. Comput. Meth. Eng. 28 (2021) 4549–4571.

[4] S.M.J. Spence, M. Gioffrè, A. Kareem, An efficient framework for the reliability-based design optimization of large-scale uncertain and stochastic linear systems, Probab. Eng. Mech. 44 (2016) 174–182.

[5] D.J. Jerez, H.A. Jensen, M. Beer, Reliability-based design optimization of structural systems under stochastic excitation: an overview, Mech. Syst. Sig. Process. 166 (2022), 108397.

[6] S.E. Gano, J.E. Renaud, J.D. Martin, T.W. Simpson, Update strategies for kriging models used in variable fidelity optimization, Struct. Multidiscip. Optim. 32 (2006) 287–298.

[7] K. Tian, P. Lai, Y. Sun, W. Sun, Z. Cheng, B. Wang, Efficient buckling analysis and optimization method for rotationally periodic stiffened shells accelerated by Bloch wave method, Eng. Struct. 276 (2023), 115395.

[8] R. Teixeira, M. Nogal, A. O'Connor, Adaptive approaches in metamodel-based reliability analysis: a review, Struct. Saf. 89 (2021), 102019.

[9] A. Sofi, E. Romeo, A unified response surface framework for the interval and stochastic finite element analysis of structures with uncertain parameters, Probab. Eng. Mech. 54 (2018) 25–36.

[10] L. Hong, B. Shang, S. Li, H. Li, J. Cheng, Portfolio allocation strategy for active learning Kriging-based structural reliability analysis, Comput. Meth. Appl. Mech. Eng. 412 (2023), 116066.

[11] S. Lee, Monte Carlo simulation using support vector machine and kernel density for failure probability estimation, Reliab. Eng. Syst. Saf. 209 (2021), 107481.

[12] J. Wang, C. Li, G. Xu, Y. Li, A. Kareem, Efficient structural reliability analysis based on adaptive Bayesian support vector regression, Comput. Meth. Appl. Mech. Eng. 387 (2021), 114172.

[13] V. Papadopoulos, D.G. Giovanis, N.D. Lagaros, M. Papadrakakis, Accelerated subset simulation with neural networks for reliability analysis, Comput. Meth. Appl. Mech. Eng. 223–224 (2012) 70–80.

[14] M. Papadrakakis, N.D. Lagaros, Reliability-based structural optimization using neural networks and Monte Carlo simulation, Comput. Meth. Appl. Mech. Eng. 191 (2002) 3491–3507.

[15] Y. Jin, H. Wang, T. Chugh, D. Guo, K. Miettinen, Data-driven evolutionary optimization: an overview and case studies, IEEE Trans. Evol. Comput. 23 (2019) 442–458.

[16] A. Chandrasekhar, K. Suresh, TOuNN: topology optimization using neural networks, Struct. Multidiscip. Optim. 63 (2021) 1135–1149.

[17] W. He, G. Li, C. Zhong, Y. Wang, A novel data-driven sparse polynomial chaos expansion for high-dimensional problems based on active subspace and sparse Bayesian learning, Struct. Multidiscip. Optim. 66 (2023) 29.

[18] S. Yang, H. Jo, K. Lee, I. Lee, Expected system improvement (ESI): a new learning function for system reliability analysis, Reliab. Eng. Syst. Saf. 222 (2022), 108449.

[19] V. Picheny, T. Wagner, D. Ginsbourger, A benchmark of kriging-based infill criteria for noisy optimization, Struct. Multidiscip. Optim. 48 (2013) 607–626.

[20] B. Gaspar, A.P. Teixeira, C.G. Soares, Assessment of the efficiency of Kriging surrogate models for structural reliability analysis, Probab. Eng. Mech. 37 (2014) 24–34.

[21] J. Zhang, M. Xiao, L. Gao, S. Chu, A bounding-limit-state-surface-based active learning Kriging method for hybrid reliability analysis under random and probability-box variables, Mech. Syst. Sig. Process. 134 (2019), 106310.

[22] K. Yuan, N.C. Xiao, Z. Wang, K. Shang, System reliability analysis by combining structure function and active learning Kriging model, Reliab. Eng. Syst. Saf. (2019), 106734.

[23] N.C. Xiao, M.J. Zuo, C. Zhou, A new adaptive sequential sampling method to construct surrogate models for efficient reliability analysis, Reliab. Eng. Syst. Saf. 169 (2018) 330–338.

[24] N. Lelièvre, P. Beaurepaire, C. Mattrand, N. Gayton, AK-MCSi: a Kriging-based method to deal with small failure probabilities and time-consuming models, Struct. Saf. 73 (2018) 1–11.

[25] B. Echard, N. Gayton, M. Lemaire, AK-MCS: an active learning reliability method combining Kriging and Monte Carlo simulation, Struct. Saf. 33 (2011) 145–154.

[26] E. Raponi, M. Bujny, M. Olhofer, N. Aulig, S. Boria, F. Duddeck, Kriging-assisted topology optimization of crash structures, Comput. Meth. Appl. Mech. Eng. 348 (2019) 730–752.

[27] T. Zafar, Y. Zhang, Z. Wang, An efficient Kriging based method for time-dependent reliability based robust design optimization via evolutionary algorithm, Comput. Meth. Appl. Mech. Eng. 372 (2020), 113386.

[28] D.R. Jones, M. Schonlau, W.J. Welch, Efficient global optimization of expensive black-box functions, J. Global Optim. 13 (1998) 455–492.

[29] M.A. Osborne, R. Garnett, S.J. Roberts, Gaussian processes for global optimization, in: Proceedings of the 3rd International Conference On Learning And Intelligent Optimization (LION3, Citeseer, 2009, pp. 1–15.

[30] D. Huang, T.T. Allen, W.I. Notz, N. Zeng, Global optimization of stochastic black-box systems via sequential Kriging meta-models, J. Global Optim. 34 (2006) 441–466.

[31] V. Picheny, D. Ginsbourger, Y. Richet, G. Caplin, Quantile-based optimization of noisy computer experiments with tunable precision, Technometrics 55 (2013) 2–13.

[32] W. Scott, P. Frazier, W. Powell, The correlated knowledge gradient for simulation optimization of continuous parameters using gaussian process regression, SIAM J. Optim. 21 (2011) 996–1026.

[33] L. Chen, H. Qiu, L. Gao, C. Jiang, Z. Yang, Optimization of expensive black-box problems via Gradient-enhanced Kriging, Comput. Meth. Appl. Mech. Eng. 362 (2020), 112861.

[34] J. Xing, Y. Luo, Z. Gao, A global optimization strategy based on the Kriging surrogate model and parallel computing, Struct. Multidiscip. Optim. 62 (2020) 405–417.

[35] M. Moustapha, B. Sudret, J.M. Bourinet, B. Guillaume, Quantile-based optimization under uncertainties using adaptive Kriging surrogate models, Struct. Multidiscip. Optim. 54 (2016) 1403–1421.

[36] J. Villemonteix, E. Vazquez, E. Walter, An informational approach to the global optimization of expensive-to-evaluate functions, J. Global Optim. 44 (2009) 509–534.

[37] Y. Pang, Y. Wang, X. Lai, S. Zhang, P. Liang, X. Song, Enhanced Kriging leave-one-out cross-validation in improving model estimation and optimization, Comput. Meth. Appl. Mech. Eng. 414 (2023), 116194.

[38] Z. Song, H. Wang, C. He, Y. Jin, A Kriging-assisted two-archive evolutionary algorithm for expensive many-objective optimization, IEEE Trans. Evol. Comput. 25 (2021) 1013–1027.

[39] H. Dong, P. Wang, C. Fu, B. Song, Kriging-assisted teaching-learning-based optimization (KTLBO) to solve computationally expensive constrained problems, Inf. Sci. 556 (2021) 404–435.

[40] M.A. Juliani, W.J.S. Gomes, An efficient Kriging-based framework for computationally demanding constrained structural optimization problems, Struct. Multidiscip. Optim. 65 (2021) 4.

[41] J.M. Parr, A.J. Keane, A.I.J. Forrester, C.M.E. Holden, Infill sampling criteria for surrogate-based optimization with constraint handling, Eng. Optim. 44 (2012) 1147–1166.

[42] Q. Zhou, Y. Wang, S.K. Choi, P. Jiang, X. Shao, J. Hu, A sequential multi-fidelity metamodeling approach for data regression, Knowl. Based Syst. 134 (2017) 199–212.

[43] J. Cheng, P. Jiang, Q. Zhou, J. Hu, T. Yu, L. Shu, X. Shao, A lower confidence bounding approach based on the coefficient of variation for expensive global design optimization, Eng. Comput. 36 (2019) 830–849.

[44] C. Jiang, Z. Hu, Y. Liu, Z.P. Mourelatos, D. Gorsich, P. Jayakumar, A sequential calibration and validation framework for model uncertainty quantification and reduction, Comput. Meth. Appl. Mech. Eng. 368 (2020), 113172.

[45] B. Keshtegar, S. Chakraborty, A hybrid self-adaptive conjugate first order reliability method for robust structural reliability analysis, Appl. Math. Modell. 53 (2018) 319–332.

[46] Y. Jung, H. Cho, I. Lee, Intelligent initial point selection for MPP search in reliability-based design optimization, Struct. Multidiscip. Optim. 62 (2020) 1809–1820.

[47] X. Du, W. Chen, Sequential optimization and reliability assessment method for efficient probabilistic design, J. Mech. Des. 126 (2004) 225–233.

[48] T.H. Lee, J.J. Jung, A sampling technique enhancing accuracy and efficiency of metamodel-based RBDO: constraint boundary sampling, Comput. Struct. 86 (2008) 1463–1476.

[49] B.J. Bichon, M.S. Eldred, L.P. Swiler, S. Mahadevan, J.M. McFarland, Efficient global reliability analysis for nonlinear implicit performance functions, AIAA J. 46 (2008) 2459–2468.

[50] B.J. Bichon, M.S. Eldred, S. Mahadevan, J.M. McFarland, Efficient global surrogate modeling for reliability-based design optimization, J. Mech. Des. 135 (2012), 011009.

[51] X. Yang, Y. Liu, Y. Gao, Y. Zhang, Z. Gao, An active learning kriging model for hybrid reliability analysis with both random and interval variables, Struct. Multidiscip. Optim. 51 (2014) 1003–1016.

[52] M. Xiao, J. Zhang, L. Gao, A system active learning Kriging method for system reliability-based design optimization with a multiple response model, Reliab. Eng. Syst. Saf. 199 (2020), 106935.

[53] N.C. Xiao, K. Yuan, H. Zhan, System reliability analysis based on dependent Kriging predictions and parallel learning strategy, Reliab. Eng. Syst. Saf. 218 (2022), 108083.

[54] H. Wu, Z. Zhu, X. Du, System reliability analysis with autocorrelated Kriging predictions, J. Mech. Des. (2020) 142.

[55] M. Yang, D. Zhang, F. Wang, X. Han, Efficient local adaptive Kriging approximation method with single-loop strategy for reliability-based design optimization, Comput. Meth. Appl. Mech. Eng. 390 (2022), 114462.

[56] D. Wang, D. Zhang, Y. Meng, M. Yang, C. Meng, X. Han, Q. Li, AK-HRn: an efficient adaptive Kriging-based n-hypersphere rings method for structural reliability analysis, Comput. Meth. Appl. Mech. Eng. 414 (2023), 116146.

[57] H.M. Kroetz, M. Moustapha, A.T. Beck, B. Sudret, A two-level Kriging-based approach with active learning for solving time-variant risk optimization problems, Reliab. Eng. Syst. Saf. 203 (2020), 107033.

[58] K. Khorramian, F. Oudah, New learning functions for active learning Kriging reliability analysis using a probabilistic approach: KO and WKO functions, Struct. Multidiscip. Optim. 66 (2023) 177.

[59] R. Teixeira, M. Nogal, A. O'Connor, B. Martinez-Pastor, Reliability assessment with density scanned adaptive Kriging, Reliab. Eng. Syst. Saf. 199 (2020), 106908.

[60] Z. Meng, Z.H. Zhang, D.Q. Zhang, D.X. Yang, An active learning method combining Kriging and accelerated chaotic single loop approach (AK-ACSLA) for reliability-based design optimization, Comput. Meth. Appl. Mech. Eng. 357 (2019), 112570.

[61] D. Meng, S. Yang, A.M.P. De Jesus, T. Fazeres-Ferradosa, S.P. Zhu, A novel hybrid adaptive Kriging and water cycle algorithm for reliability-based design and optimization strategy: application in offshore wind turbine monopile, Comput. Meth. Appl. Mech. Eng. 412 (2023), 116083.

[62] M. Papadrakakis, N.D. Lagaros, Y. Tsompanakis, V. Plevris, Large scale structural optimization: computational methods and optimization algorithms, Arch. Comput. Meth. Eng. 8 (2001) 239–301.

[63] A.J. Torii, R.H. Lopez, L.F. Miguel, A general RBDO decoupling approach for different reliability analysis methods, Struct. Multidiscip. Optim. 54 (2016) 317–332.

[64] J. Thedy, K.W. Liao, Reliability-based structural optimization using adaptive neural network multisphere importance sampling, Struct. Multidiscip. Optim. 66 (2023) 119.

[65] B. Gaspar, A.P. Teixeira, C.G. Soares, Adaptive surrogate model with active refinement combining Kriging and a trust region method, Reliab. Eng. Syst. Saf. 165 (2017) 277–291.

[66] Z. Zhao, Z.H. Lu, Y.G. Zhao, A Kriging-assisted two-stage adaptive radial-based importance sampling method for random-interval hybrid reliability analysis, Struct. Multidiscip. Optim. 66 (2023) 136.

[67] S.N. Lophaven, H.B. Nielsen, J. Søndergaard. DACE-A Matlab Kriging toolbox, 2002, version 2.0. http://www.imm.dtu.dk/pubdb/p.php?3213.

[68] Y. Zhai, P. Han, Data integration with oracle use of external information from heterogeneous populations, J. Comput. Graph. Statist. 31 (2022) 1001–1012.

[69] M.B. Oguntola, R.J. Lorentzen, Ensemble-based constrained optimization using an exterior penalty method, J. Pet. Sci. Eng. 207 (2021) 109165.

[70] R.B. Gramacy, G.A. Gray, SLe Digabel, H.K.H. Lee, P. Ranjan, G. Wells, S.M. Wild, Modeling an Augmented Lagrangian for Blackbox Constrained Optimization, Technometrics 58 (2016) 1–11.

[71] E. Burman, P. Hansbo, M.G. Larson, The augmented lagrangian method as a framework for stabilised methods in computational mechanics, Arch. Comput. Meth. Eng. 30 (2023) 2579–2604.

[72] Z. Meng, Z.H. Zhang, G. Li, D.Q. Zhang, An active weight learning method for efficient reliability assessment with small failure probability, Struct. Multidiscip. Optim. 61 (2020) 1157–1170.

[73] Y. Aoues, A. Chateauneuf, Benchmark study of numerical methods for reliability-based design optimization, Struct. Multidiscip. Optim. 41 (2010) 277–294.

[74] A. Okoro, F. Khan, S. Ahmed, Dependency effect on the reliability-based design optimization of complex offshore structure, Reliab. Eng. Syst. Saf. 231 (2023), 109026.

[75] B.D. Youn, K.K. Choi, L. Du, Enriched performance measure approach for reliability-based design optimization, AIAA J. 43 (2005) 874–884.

[76] T.M. Cho, B.C. Lee, Reliability-based design optimization using convex linearization and sequential optimization and reliability assessment method, Struct. Saf. 33 (2011) 42–50.

[77] W. Fauriat, N. Gayton, AK-SYS: an adaptation of the AK-MCS method for system reliability, Reliab. Eng. Syst. Saf. 123 (2014) 137–144.

[78] K. Svanberg, The method of moving asymptotes-a new method for structural optimization, Int. J. Numer. Methods Eng. 24 (1987) 359–373.

[79] J. Yi, Q. Zhou, Y. Cheng, J. Liu, Efficient adaptive Kriging-based reliability analysis combining new learning function and error-based stopping criterion, Struct Multidisc Optim 62 (2020) 2517–2536.

[80] I. Lee, K.K. Choi, D. Gorsich, Sensitivity analyses of FORM-based and DRM-based performance measure approach (PMA) for reliability-based design optimization (RBDO), Int. J. Numer. Methods Eng. 82 (2010) 26–46.

[81] R. Biswas, D. Sharma, A single-loop shifting vector method with conjugate gradient search for reliability-based design optimization, Eng. Optim. 53 (2021) 1044–1063.

[82] S.B. Jeong, G.J. Park, Single loop single vector approach using the conjugate gradient in reliability based design optimization, Struct. Multidiscip. Optim. 55 (2017) 1329–1344.

[83] S. Arunachalam, S.M.J. Spence, An efficient stratified sampling scheme for the simultaneous estimation of small failure probabilities in wind engineering applications, Struct. Saf. 101 (2023), 102310.

[84] X. Yang, Y. Liu, Y. Zhang, Z. Yue, Probability and convex set hybrid reliability analysis based on active learning Kriging model, Appl. Math. Modell. 39 (2015) 3954–3971.

[85] J. Zhang, M. Xiao, L. Gao, A new local update-based method for reliability-based design optimization, Eng. Comput. 37 (2021) 3591–3603.

[86] D. Lee, S. Rahman, Reliability-based design optimization under dependent random variables by a generalized polynomial chaos expansion, Struct. Multidiscip. Optim. 65 (2021) 21.

[87] M. Ilchi Ghazaan, F. Saadatmand, Decoupled reliability-based design optimization with a double-step modified adaptive chaos control approach, Struct. Multidiscip. Optim. 65 (2022) 284.

[88] Z. Meng, C. Li, P. Hao, Unified reliability-based design optimization with probabilistic, uncertain-but-bounded and fuzzy variables, Comput. Meth. Appl. Mech. Eng. 407 (2023), 115925.